



Babes-Bolyai University

Faculty of Chemistry and Chemical Engineering



Extended summary of the Ph.D. Thesis

Computational studies with practical applications

Ph.D. Student

Szilárd-Zoltán Pesek

Scientific advisor:

Prof. Dr. Radu Silaghi-Dumitrescu

Cluj-Napoca

2023

Contents of the thesis

1. Introduction	Error! Bookmark not defined.
2. The iodine / iodide / starch supramolecular complex	Error! Bookmark not defined.
2.1. Introduction.....	Error! Bookmark not defined.
2.1.1. General considerations of reaction starch with iodine	Error! Bookmark not defined.
2.1.2. Dependence on the nature of the organic (bio)polymer	Error! Bookmark not defined.
2.1.3. Geometrical data	Error! Bookmark not defined.
2.1.4. The I ₂ -only hypothesis	Error! Bookmark not defined.
2.1.5. Poly-iodine anions as candidates	Error! Bookmark not defined.
2.1.6. Structural role of water	Error! Bookmark not defined.
2.1.7. Scope of the present study	Error! Bookmark not defined.
2.2. Materials and Methods.....	Error! Bookmark not defined.
2.3. Results and Discussion	Error! Bookmark not defined.
2.3.1. Amylose-iodine/iodide complexes: structural considerations	Error! Bookmark not defined.
2.3.2. UV-vis simulations of linear I ₂ chains	Error! Bookmark not defined.
2.3.3. UV-vis simulations of linear I _n ⁻ systems.....	Error! Bookmark not defined.
2.3.4. UV-vis simulations of linear I _n ⁻ -I ₂ systems	Error! Bookmark not defined.
2.3.5. Solvent effects.....	Error! Bookmark not defined.
2.4. Conclusions.....	Error! Bookmark not defined.
3. Analysis of supramolecular organization in polylactic acid (PLA)	Error! Bookmark not defined.
3.1. Introduction.....	Error! Bookmark not defined.
3.2. Materials and Methods.....	Error! Bookmark not defined.
3.3. Results and Discussion	Error! Bookmark not defined.
3.3.1. Supramolecular interactions between PLA chains.....	Error! Bookmark not defined.
3.3.2. Comparison of protein-like structures with the De Santis experimental structure.....	Error! Bookmark not defined.
3.3.3. Conclusions.....	Error! Bookmark not defined.
3.3.4. Ramachandran analysis of optimized PLA structures.....	Error! Bookmark not defined.
3.3.5. Conclusions.....	Error! Bookmark not defined.
4. Computational contributions to understanding the removal and degradation of sodium diclofenac via radical-based mechanism using <i>S. sclerotiorum</i> laccase	Error! Bookmark not defined.
4.1. Introduction.....	Error! Bookmark not defined.
4.1.1. UV-vis analysis of diclofenac oxidation by laccase.....	Error! Bookmark not defined.
4.1.2. EPR analysis	Error! Bookmark not defined.

4.1.3. Mass spectra and structure assignment	Error! Bookmark not defined.
4.2. Materials and Methods	Error! Bookmark not defined.
4.3. Results and discussion	Error! Bookmark not defined.
4.3.1. Characterization of the laccase-induced precipitate	Error! Bookmark not defined.
4.4. Conclusions	Error! Bookmark not defined.
5. Prediction of UV-vis and fluorescence properties in a series of phenathiazonium derivatives	
Error! Bookmark not defined.	
5.1. Introduction	Error! Bookmark not defined.
5.2. Materials and methods	Error! Bookmark not defined.
5.3. Results and Discussion	Error! Bookmark not defined.
5.4. Conclusions	Error! Bookmark not defined.
6. DFT evaluation of the spectrochemical series	Error! Bookmark not defined.
6.1. Introduction	Error! Bookmark not defined.
6.1.1. Crystal and ligand field theory	Error! Bookmark not defined.
6.1.2. The spectrochemical series	Error! Bookmark not defined.
6.1.3. Confounding factors affecting the spectrochemical series: covalence, nephelauxetic effect, Racah parameters	Error! Bookmark not defined.
6.2. Materials and methods	Error! Bookmark not defined.
6.3. Results and discussion	Error! Bookmark not defined.
6.4. Conclusions	Error! Bookmark not defined.
7. Conclusions	Error! Bookmark not defined.
8. References	Error! Bookmark not defined.
9. List of publications and conference participations	Error! Bookmark not defined.
10. Supporting Information	Error! Bookmark not defined.
10.1. For Chapter 2: On the origin of the blue color in the iodine / iodide / starch supramolecular complex	Error! Bookmark not defined.
10.2. For Chapter 3: Analysis of supramolecular organization in polylactic acid (PLA)	Error! Bookmark not defined.
10.3. For Chapter 4: Removal and degradation of sodium diclofenac via radical-based mechanism using <i>S. sclerotiorum</i> laccase	Error! Bookmark not defined.
10.3.1. Materials and methods	Error! Bookmark not defined.
10.3.2. Enzymatic characterization of the laccase-diclofenac system.	Error! Bookmark not defined.
10.4. For Chapter 5: Prediction of UV-vis and fluorescence properties in a series of phenathiazonium derivatives	Error! Bookmark not defined.
10.5. For Chapter 6: DFT evaluation of the spectrochemical series	Error! Bookmark not defined.

Contents of the summary

Keywords: *starch, polymer, complex, polylactic acid, structure, diclofenac, phenathiazonium, DFT, spectrochemical* 4

- 1. Introduction** 5
- 2. The iodine / iodide / starch supramolecular complex** 7
- 3. Analysis of supramolecular organization in polylactic acid (PLA)** 14
- 4. Computational contributions to understanding the removal and degradation of sodium diclofenac via radical-based mechanism using *S. sclerotiorum* laccase** 18
- 5. Prediction of UV-vis and fluorescence properties in a series of phenathiazonium derivatives** 22
- 6. DFT evaluation of the spectrochemical series** 26
- 7. Conclusions** 30

References 32

Keywords: *starch, polymer, complex, polylactic acid, structure, diclofenac, phenathiazonium, DFT, spectrochemical*

1. Introduction

The needs of today's society have led to the transformation of the entire teaching-learning-evaluation process into a more alert pace, based on the development of technologies and the evolution of the educational paradigm. Thus, the mission of the educational system is to use effective strategies for the formation of competence in the use of information technologies, from simple operations to the possibility of the manifestation of creative elements and the development of new intellectual products. The development of these specific skills allows a more flexible adaptation to the major changes occurring in our century having a favorable impact on the use of computing information technologies in everyday life.

The design of modern didactic activity in the discipline of chemistry, in the context of current changes, requires a new structure, imposed both by the new requirements of the school curriculum and by the desire of students and teachers to use modern informational means in the instructional-educational process.

By studying chemistry, the development of digital skills is pursued, in the field of information and communication technologies. Thus, competences are formed in the use of tools with digital action in real situations and competences in the creation of documents in the communicative, informational field and the use of electronic services, including the Internet, in real situations.

The use of these informational technologies in chemistry presents several advantages, among which I would like to mention: the diversification of teaching strategies, the stimulation of interest in something new, the motivation of learning through images of objects related to everyday life, through chemical video experiences, the possibility of viewing them as many times as possible necessary; the possibility of simulating chemical phenomena, of using animated and dynamic images, facilitating the learning of chemistry curriculum content; the use of virtual laboratories for experimental computer activities; the integration of knowledge by carrying out individual and group projects; providing effective mechanisms for differentiated and individualized education; creating your own professional development path, etc.

Recent studies prove interdisciplinary links between Chemistry-Physics-Biology that can be extended to other fields based on additional tasks. Therefore, in the case of students carrying out research projects, transdisciplinary objectives can be achieved, having a beneficial influence on the formation of professional competence.

The integration of objectives from the field of chemistry with solutions from the field of information technologies or other fields, indisputably represents new opportunities in addressing complicated problems. All of this supports the development of the research skills of concrete phenomena, contributing to the motivation for training, the increase of school performance and the training of specialists capable of proposing novel solutions.

New information technologies, and implicitly computational modelling, are not just a tool to present existing content in a different way. They must lead to the modification of the way of thinking and the style of working with the class of the teachers.

The present thesis attempts to employ the modern tools of computational chemistry in order to illustrate applications on issues of very general interest, that may be translatable or relatable for pre-college and early-college students. Four topics are chosen for computational exploration. The first one is the very common iodine-starch color reaction - a tool present in the earliest of the laboratory experiments in schools, as well as throughout many analytical procedures taught in undergraduate classes. Yet, the very mechanism of this reaction is still unclear; this thesis reports computations, accompanied by some experiments, that may provide a convincing mechanism that reconciles previous apparent conflicts between experiment and theory. These calculations entail predictions of spectroscopic properties (or, more simply put, color – simulated with time-dependent density functional calculations, TD-DFT) as well as supramolecular architectures of oligo/poly-saccharide and of poly-halide chains. A second topic treated in the thesis is the nature of secondary and supramolecular structure in a biopolymer of practical interest, polylactic acid; this chapter of the thesis expands upon previous work by PhD student Izabela Irsai and has a focus on the influence of weak intra- and inter-molecular interactions on the general shape/conformation of the molecules. A third topic of the thesis entails exemplification of the use of computational chemistry in assigning the identity of reaction products from complex reaction mixtures in a process of general interest/perspectives, namely bioremediation of water contaminated with a medical compound, diclofenac. Here, again, TD-DFT calculations are main tool. A fourth chapter resorts to TD-DFT calculations in order to rationalize and predict subtle variations in color and in fluorescence between a series of organic compounds. The fifth chapter returns to the inorganic stage also illustrated by the poly-iodide chains of the first chapter, and now discusses a topic of general interest in transition metal chemistry, namely the spectrochemical series. DFT calculations and molecular orbital analyses are employed, in an attempt to systematically explore the validity and applicability of this well-known basic tool of

coordination chemistry, and to rationalize its subtle variations vs. experiments as well as between various types of metal centers.

2. The iodine / iodide / starch supramolecular complex¹

Amylose is a linear polymer typically containing 300-3000 (or sometimes much more) monomeric units, always bound via $\alpha(1\rightarrow4)$ glycosidic bonds (cf. **Error! Reference source not found.**)¹. Amylopectin has a similar structure, additionally features ramifications via $\alpha(1\rightarrow6)$ bonds. Both polymers are sparsely soluble in water – with amylose more so than amylopectin. Inside living organisms, the enzyme amylase is mainly responsible for hydrolyzing starch. Dextrins, which are polysaccharides with a low degree of polymerization, are produced by partial hydrolysis of starch; with complete hydrolysis, glucose is formed.²

Amylose can exist in a disordered amorphous conformation or in two different helical forms. It can form a double helix with itself (the A or B form) or it can bind with another hydrophobic guest molecule such as iodine, a fatty acid or an aromatic compound and is known as the V form (cf. Figure 2. 1.). The polysaccharide chain of V-amylose found naturally in the non-A and non-B segments of amylose contains 6 glucose units per turn with a step height of 7.91 to 8.17 Å⁷⁻⁹ and forms a similar central cavity channel, being folded into a single left spiral. The V form can be isolated by precipitation from aqueous solution using alcohols, ketones, fatty acids, iodine or salts that form inclusion complexes. The properties thus found are similar to those found in related cyclodextrins, α -cyclodextrin or cyclohexaamylose (CA6).^{14,15}.

¹ This chapter is published as Pesek, Szilard, Lehene, Maria; Branzanic, Adrian M. V.; Silaghi-Dumitrescu, Radu. On the origin of the blue color in the iodine / iodide / starch supramolecular complex. *Molecules*, 2022, 27(24), 8974; <https://doi.org/10.3390/molecules27248974> and a follow-up review Silaghi-Dumitrescu, R.; Pesek, S. The Iodine/Iodide/Starch Supramolecular Complex. *Preprints* 2023, 2023081380. <https://doi.org/10.20944/preprints202308.1380.v1>

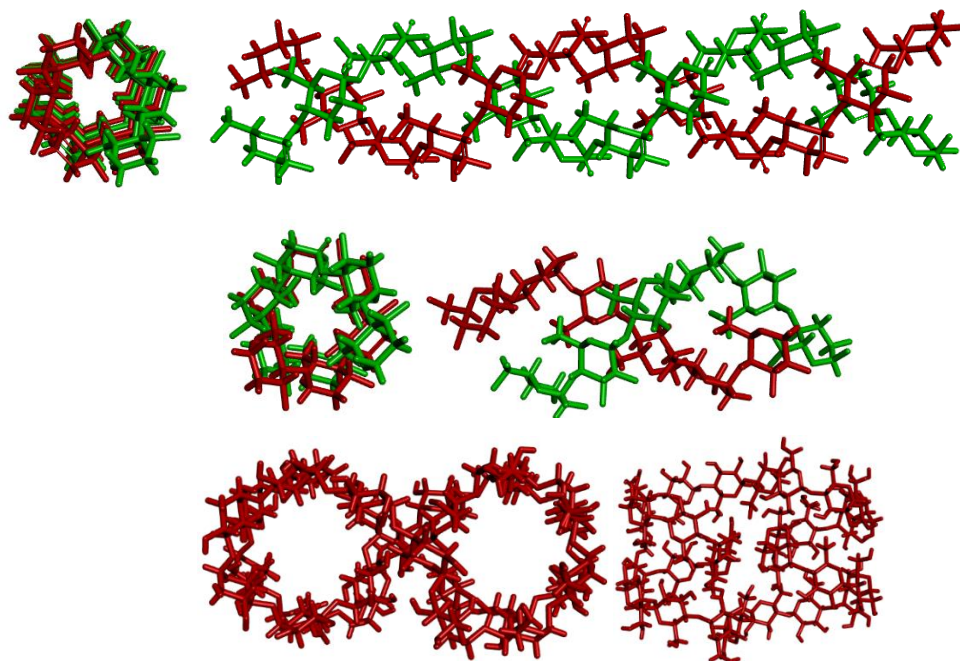


Figure 2. 1. Molecular models of helices of (a) A-type, B-type and of V-type cycloamylose.

Amylose V is the allomorph known for its deep blue complexes with iodine. The iodine molecules are caught in the canals within the helices, where also molecules of the solvent can be present. The nature of the blue complex of amylose with iodine has been a focus of research for many decades.²² The stoichiometry and charge of the poly-iodine substructures of the starch-iodine complex is still disputed. However, it is now generally accepted that iodide ions are also required in the process, so that the poly-iodine chains inside the amylose helix consist of a mixture/combination of I_2 and I^- ^{22–28} with an unusual metallic-like structure.²⁹

This chapter of the thesis reports an experimental and computational study of the amylose-iodine-iodide system, using UV-vis spectra, time-dependent density functional theory (TD-DFT), semiempirical and molecular mechanics calculations in order to model the structure of the complex and to assess the viability of various candidates potentially responsible for the blue color. Poly- I_2 as well as I_n^- structures are examined.

I_2 alone, either in aqueous or in alcoholic solutions (methanol or ethanol) leads to barely detectable changes in absorbance at ~600 nm in reaction with starch. Iodine-iodide mixtures do yield a blue color, which is not observed with glucose instead of starch. The absorbance maximum of the iodine-iodide-starch complex in the experiments reported in **Error! Reference source not found..** and **Error! Reference source not found..** is at ~580 nm. This is slightly different from the 615 nm reported for amylose – but is in line with the fact that our starch samples also contain amylopectin, as well as with the fact that the precise

position of the maximum depends on the source of the starch as well as on the relative concentrations of the reagents.^{24,26,41-44} Indeed, slight concentration dependent changes of the position of the maximum are observed when varying the iodide concentration as well as when varying the length of the amylose/amylopectin chains by employing an amylase.

Binding of I₂ to the helix (model A-I₂ in Table 2. 1. and Figure 2. 2.) leads to smaller distortions of the helix than water (1% and 4%, respectively, for the length and the diameter). The non-polar character of I₂ may be held responsible for this difference. The interaction energy per I₂ molecule is essentially negligible (cf. Supporting Information), as expected in line with the fact that the amylose helix does not serve to stabilize the I₂ molecules by noncovalent sugar-I₂ interactions, but rather to provide a less hydrophobic medium for the iodine molecules.

Binding of interspersed water and iodine molecules (model A-I₂-H₂O) results in distortions closer to the A-H₂O model (3% increase in length, 10% in diameter), perhaps in line with the fact that the water molecules again migrate to the internal walls of the helix. The total interaction energy between the amylose and the 3 I₂ and 4 H₂O units in A-I₂-H₂O is only ~5 kcal/mol – thus suggesting that water-iodine mixtures are an unlikely mixture to be found at the interior of the amylose helix. Moreover, and more importantly, given the strong amylose-water interactions seen in the A-H₂O model, it can be expected that I₂ molecules alone would be unable to dislocate water molecules from inside the amylose helix. This may explain why I₂ has been shown to efficiently bind to amylose in dry/solid state, but much less so in solution (unless special conditions, e.g. heating) are provided.⁴⁵

Table 2. 1. Key distances (Å) derived computed for iodine-amylose models. The starting geometry of the A models featured a length of 32.69 Å and a diameter of 7.04 Å.

Model	Helix length	Helix diameter	I-I distances
I ₂	-	-	2.54
I ₃ ⁻	-	-	2.62
(I ₂) ₃	-	-	Intramolecular: 2.55 / 2.55 / 2.55 Intermolecular: 2.94 / 2.94
A	32.90	7.15	-
A-H ₂ O	34.38	7.82	-
A-I ₂	33.08	7.44	Intramolecular: 2.55 / 2.56 / 2.56 / 2.56 / 2.56 / 2.56 / 2.55 Intermolecular: 2.85 / 2.84 / 2.84 / 2.83 / 2.83 / 2.84
A-I ₂ -H ₂ O	34.00	7.89	Intramolecular: 2.65 / 2.65 / 2.65 Inter-I ₂ : 7.60 / 5.80 H ₂ O-I: 4.56 / 5.09 / 3.92 / 3.92 / 3.79 / 3.93
A-I ₃ ⁻	34.04	7.14	2.65 / 2.65

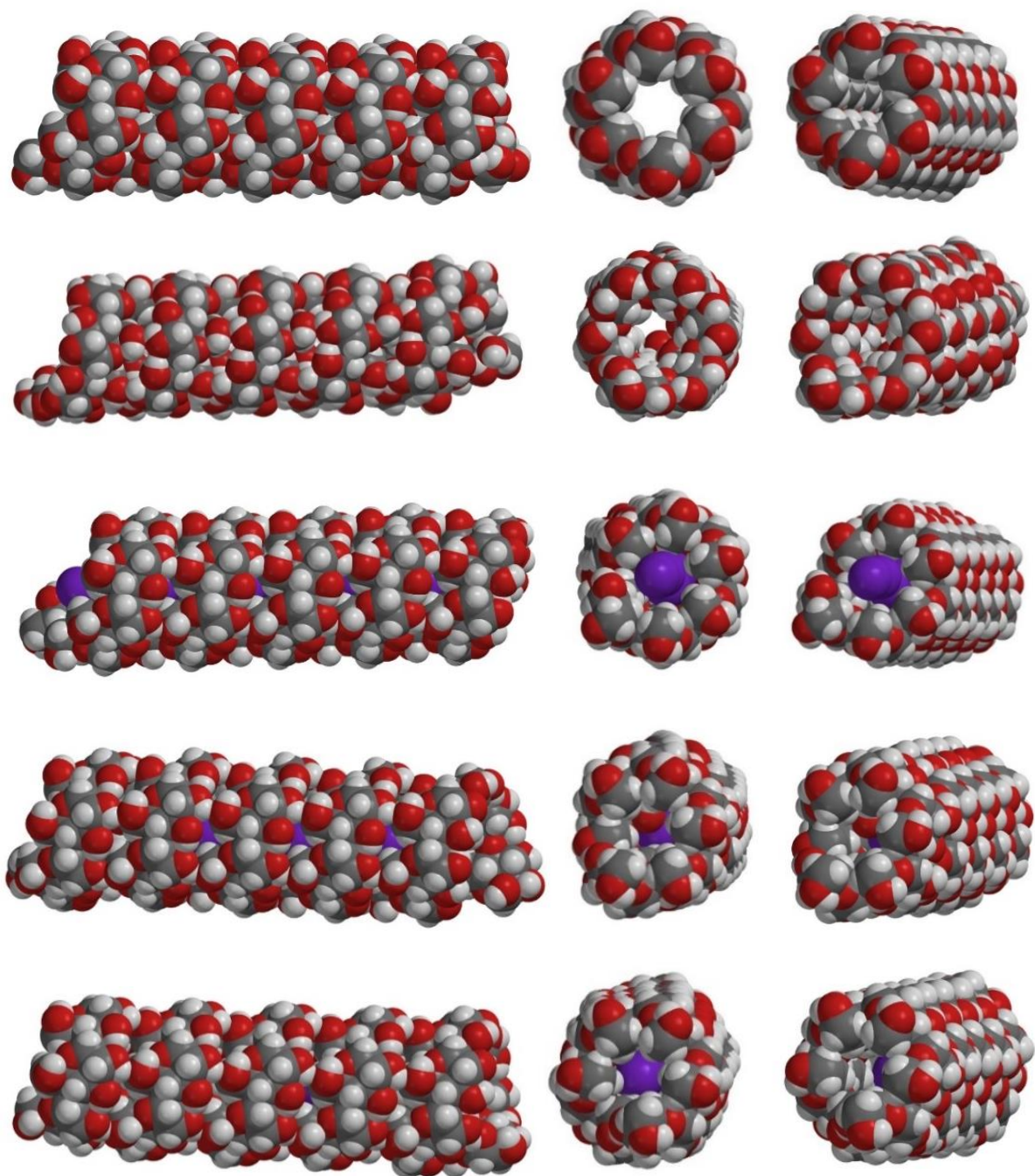










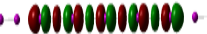

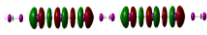



Figure 2. 2. Structures of AM1-optimized amylose models, in order of rows: A, A-H₂O, A-I₂, A-I₂-H₂O, A-I₃.

Table 2. 2. I-I distances (Å), wavelengths for the major maximum in the visible region (nm), oscillator strengths (OS) and relevant molecular orbitals on linear I_nI₂ models from TD-DFT (B3LYP/def2-SV(P)) calculations. Data shown in italics are for structures built with intramolecular I-I distances known experimentally for I₂ in solid state (2.72 Å), and with intermolecular distances arbitrarily set at 4.05 Å (i.e., at the limit of the sum of van der Waals radii) – without any further geometry optimization. All other data are from fully optimized geometries.

Model	Distance	Wavelength	OS	Orbitals	
I ₂ -I ₃ I ₂	2.72,4.05	680	1.5507	HOMO -2 (86) 	LUMO (89) 
I ₂ -I ₃ I ₂	2.80, 3.36, 3.00, 3.00, 3.36, 2.80	479	3.7407	HOMO -4 (84) 	LUMO (89) 
I ₂ -I ₅ I ₂	2.72, 4.05	681	1.9297	HOMO -4 (109) 	LUMO (114) 
I ₂ -I ₅ I ₂	2.76, 3.57, 2.89, 3.13, 3.13, 2.89, 3.57, 2.76	576	3.8021	HOMO -4 (109) 	LUMO (114) 
I ₂ -I ₇ I ₂	2.72, 4.05	666	2.6088	HOMO -4 (134) 	LUMO (139) 
I ₂ -I ₉ I ₂	2.72, 4.05	655	3.9582	HOMO -6 (157) 	LUMO (164) 
I ₂ -I ₅ ⁻ I ₂ -I ₅ ⁻ I ₂	2.72, 4.05	681	2.3723	HOMO-9 (192) 	LUMO+1 (203) 

As shown by our DFT calculations., an isolated iodine molecule displays a weak maximum at ~600 nm, due to a π^* (HOMO) \rightarrow σ^* (LUMO) transition. In a linear I₂ dimer, this maximum sees a bathochromic shift and a slight increase in intensity, as expected since at such short intermolecular distance the frontier orbitals of the two I₂ molecules mix. Longer chains of I₂ molecules follow the same trends seen when going to monomeric I₂ to (I₂)₂ (including the elongation of intermolecular distances upon geometry optimization). The bathochromic and hyperchromic shifts continue to the extent that in the heptamer the intensity of the 600-nm band has ~ tripled compared to isolated iodine. These data confirm the experimental observations and previous semiempirical calculations according to which a linear chain of I₂ molecules may under certain conditions be hosted inside the amylose helix and that such a chain would display a more intense color than free iodine molecules in solution. The band responsible for this enhanced blue color entails a HOMO- \rightarrow LUMO transition, where HOMO is a combination of I₂ π^* orbitals and LUMO is a combination of I₂

σ^* orbitals. The longer the poly-I₂ chain is, the more there is a tendency for these molecular orbitals to no longer have exactly the same distribution across the same atoms – hence allowing the 600-nm band to gain a charge-transfer character which may be responsible for the increased oscillator strength. In the optimized poly-I₂ geometries, the frontier molecular orbitals responsible for the blue color are located mostly at the two ends of the chains – and it is at these ends, and at the I₂ molecules preceding the ends – that the above-mentioned charge transfer will occur. However, if the I₂ molecules are compacted together within van der Waals radii (and not further optimized), it is the center and not the edges of the poly-I₂ chain that holds the most contribution to the 600-nm band – though, again, the more important charge-transfer part will impact more clearly the iodine molecules preceding the ends of the chain. Although the above considerations may explain the amylose – I₂ interactions under certain conditions, the enhancement of the 600 nm band upon elongation of the poly-I₂ is still relatively small – not even one order of magnitude upon going from monomer to heptamer. Therefore, poly-iodine-iodide chains were considered next, as illustrated in **Error!**
Reference source not found..

The mono-anions I_n⁻ (n = 1, 5, 7, 9) tend to exhibit bands in the ~400 nm region. However, the nature and intensity of this band depends strongly on the geometry of the anion. When the anion is built with equivalent I-I distances, to mimic complete delocalization of the negative charge across the molecule, the predicted absorption band remains very weak and close to the 400 nm region. The nature of this transition remains very similar to the one seen in the poly-I₂ chains (i.e., π^* (HOMO) \rightarrow σ^* (LUMO). When the geometry of the I_n⁻ chains is optimized, the symmetry of the molecule is lost as the I-I distances no longer remain degenerate; importantly, this asymmetry allows the HOMO-LUMO transition to gain significant charge-transfer character – so much so that its intensity increases by as 3-4 orders of magnitude compared to the completely symmetrical models. These increases in intensity are also accompanied by small bathochromic shifts; however, these shifts appear confined below 500 nm and hence these polyanions of iodide do not appear to be reasonable candidates for the experimentally-observed 600-nm species. Another notable change in these geometry-optimized I_n⁻ species is that at n>3 the HOMO orbital involved in the visible transition now also has σ^* character.

Table 2. 2. shows a set of models which yield excellent agreement with experiment, insofar as featuring extremely intense bands at 600 nm. These models include any I_n^- species surrounded by two neutral I_2 molecules. In such models, the ~600 nm transition occurs from a σ^* orbital of the central oligo-iodide anion to the σ^* orbitals of the terminal I_2 molecules. For the $I_2-I_3^-I_2$ system, the formal structure featuring the I_2 molecules at van der Waals radii from the I_3^- anion does allow a very strong band at 680 nm. However, upon geometry optimization this structure collapses into the I_7^- anion, already seen in **Error! Reference source not found.** as an unlikely candidate for the blue-colored complex. No such collapse is seen for the $I_2-I_5^-I_2$ species, which is thus the first of those discussed in the present study that can be proposed as a strong candidate as a contributor to the amylose-iodine blue color. Moreover, the average iodine-iodine distances in the DFT-optimized geometry of $I_2-I_5^-I_2$ is 3.09 Å, remarkably close to the 3.1 Å distance measured experimentally for the iodine-iodide-amylose complex. As shown in

Table 2. 2., I_2 combinations with longer I_n^- species cannot be excluded.

The 600 nm band in

Table 2. 2. is predicted to shift by as much as 25 nm upon going from $n=3$ to $n=9$, while over the same interval its intensity is seen to double. Given the uncertainties regarding the exact formula of the species, reliable extinction coefficients for the amylose-iodine-iodide complex are not known;

Table 2. 2. now shows that they would be particularly difficult to measure, since poly-iodine chains of various lengths will have different extinction coefficients. On the other hand, having singled out the $I_2-I_5^-I_2$ unit as the most likely candidate of those examined in **Error! Reference source not found.. Error! Reference source not found..** and

Table 2. 2. for the “blue complex”, one may consider how longer chains of such units may behave.

Table 2. 2. therefore also shows that the homologous assembly $I_2-I_5^-I_2-I_5^-I_2$ - technically, a dimer of $I_2-I_5^-I_2$, features an absorption maximum essentially at the same wavelength as the monomer – albeit with a different extinction coefficient. As such, $I_2-I_5^-I_2$ itself, and not longer chains/polymers thereof, appears sufficient to justify the blue color of the iodine-iodide-amylose complex.

To conclude, in this chapter the amylose-iodine-iodide interaction has been modeled with electronic structure calculations. Changes in the structure of the helix upon iodine binding are predicted. Poly- I_2 structures are shown to be responsible for enhanced blue color under certain conditions (e.g., dry/solid amylose). Poly- I_n^- structures are found unlikely to exist inside the amylose helix or to be responsible for the blue color. Instead, I_2/I_n^- pairs with

charge transfer bands from the occupied I_n^- ($n>3$) σ^* to the empty $I_2 \sigma^*$ orbital are found to be reasonably responsible for the blue color. Of these, $I_2-I_5-I_2$ associations are the smallest (and possibly - but not necessarily - repetitive) unit that represent local minima in DFT calculations, with average iodine-iodine distances essentially identical to the 3.1 Å value seen experimentally in the iodine-amylose complex. The distinct charge-transfer character of the UV-vis bands also brings about a strong dependence on the dielectric constant in the region $\epsilon \sim 1 - 30$, which in turn may explain at least part of the dependence of the UV-vis properties of amylose-iodine/iodine complexes on various external factors that may subtly affect amylose architecture and hence exposure of the interior cavity to solvent (e.g., temperature, other solutes, solvents, chain length).

3. Analysis of supramolecular organization in polylactic acid (PLA)²

Lactic acid (LA) is a key metabolic intermediate in most living organisms.⁴⁶ Polylactic acid (PLA) is one of the most important biodegradable polymeric materials for industrial applications^{47,48}. LA is a chiral molecule with d- and l-type isomers, thus forming three forms of PLA: poly-l-lactic acid (PLLA), poly-d-lactic acid (PDLA) and poly-D,L-lactic acid (PDLLA)⁴⁹. The three-dimensional structure of PLA is still a matter of investigation. A series of investigations have been aimed at drawing analogies between lactic acid and aminoacids (e.g., based on the fact that LA can be viewed as an analogue of alanine where the amino group has been replaced by a hydroxyl) – posing the question whether PLA can adopt secondary (and possibly tertiary and quaternary) structural features analogous to those seen in aminoacids. Optimizations of the geometry of the secondary structure of polylactic acid (PLA), consisting of decameric units, analogous to those observed in the structure of proteins - helical structures (α , π , 3_{10}), as well as a β sheet – were reported using molecular mechanics, methods semiempirical, ab initio and density functionals. The best method used (M062x/6-311+G**) predicts that the α , π and 3_{10} structures have very similar energies, with π slightly favored by values within the error limits of the method. Furthermore, a comparison of PLLA with PDLLA revealed that the poly-L lactic acid structure is energetically favored over the PDLLA.⁵⁰

² Published as Irsai, Izabella; Pesek, Szilard, Silaghi-Dumitrescu, Radu. A critical review of computational efforts towards identifying secondary structure elements in polylactic acid (PLA). *Revue Roumaine de Chimie*, 2023, in press, and Irsai, Izabella; Pesek, Szilard, Silaghi-Dumitrescu, Radu. Polylactic acid inter-chain interactions. *Studia Universitatis Babeş-Bolyai Seria Chemia*, 2022, LXVII, 47-71 ; DOI:10.24193/subbchem.2022.4.04.

The interaction between two polylactic acid chains was also examined. PLLA structures were found to be more stable than poly(DL-lactic acid) (PDLLA) copolymers. By examining the individual structures with HF/3-21G*, the β -sheet dimer was determined to be the most stable and the π -helix dimer was found to be the least stable. As the values obtained were very close, it was difficult to determine which is the most stable geometry.⁵³ It was found that the computational predictions on the relative stabilities are dependent on the methods employed. In the case of PLLA, the α helix is predicted the most stable at empirical and semiempirical methods. The Hartree-Fock methods anticipate the most stable structure is the β -sheet. The DFT methods predict that α , π , 3_{10} helices have similar energies, in contrast with results obtained with semiempirical and empirical methods. The DFT method with the larger utilized basis set with diffuse function prefigured the most stable of the four structures examined is the π helix and the least stable is the β -sheet. There are the same discrepancies for the PDLLA as for the PLLA. Reported here is a molecular-level investigations of the inter-chain weak interactions involving PLA units, as part of an effort ultimately aiming to provide useful data for predicting and controlling macroscopic properties of PLA-based materials. Also, a critical view at the types of secondary structure in PLA chains is given. **Error! Reference source not found.** illustrates a typical dimer structure, with atom numbering further used in the Tables. The stability of the generated geometries was determined as the difference between the energy obtained during the dimer optimization and 2x the value of the energy received from the monomer optimization.

Table 3. 1. shows a summary of the data collected for the thus-calculated inter-chain interaction energies calculated per unit of lactic acid, based on the adapted from previous work by Irsai¹⁷². These values are expected to be useful in predicting interaction energies between chains of lengths different from the decameric structures examined in the present study. The weakest interactions are seen for the perpendicular structures; among those, the strongest are for π , 3_{10} , while the DeSantis structure affords no local minimum at all. The strongest interactions are seen with parallel structures – of which the largest interaction energies are with the DeSantis and the π monomers (up to 2.8 and 4.2 kcal/mol per unit of lactic acid, respectively).

Table 3. 1. Relative energies (kcal/mol) of inter-chain interactions per unit of lactic acid.

ΔE	α	π	3_{10}	β	DeSantis
Perpendicular	1.0	1.5	0.9-1.6	1.2	-

Antiparallel	1.8	2.2-3.5	0.4-0.5	1.8-3.2	1.5-1.9
Parallel	0.4-2.7	2.6-2.8	0.6-2.4	1.1-2.1	2.6-4.2

Φ and Ψ angles were then measured in the optimized geometries of α , π , 3_{10} helices, β sheet and De Santis structures of decameric PLA units. These values are listed in Table 3. 2. for the M062x data, with graphical representations in Figure 3. 1. The α , π , and 3_{10} helices all appear to display angles significantly different from the initial values – and all centered around $-60/70$ and $-20/30^\circ$. The similarity among these three optimized structures is mirrored by the similar chain lengths in **Error! Reference source not found.**, all suggesting that the three optimized structures essentially describe the same type of secondary structure. The slight energy differences in **Error! Reference source not found.** (at the M062x level of theory) are mirrored mainly by slight differences in Φ and Ψ angles at the ends of the decameric chain. The angle values are reasonably similar in all three cases to the type III β turn seen in the canonical Ramachandran peptide classification. The β sheet, after optimization, appears closer to a δ turn. The DeSantis structure, after optimization, shows no resemblance to any peptide-like structure known canonically.

Table 3. 2. ϕ and Ψ Ramachandran assignments based on angle values of the DFT optimized α helix (initial values are -58° and -47°), π helix (initial values are -57° and -70°), 3_{10} helix (initial values are -49 and -26), β sheet (initial values are 180° and 180°) and De Santis structure (initial values are -29° and 92°).

Starting canonical structure	Assignment of optimized structure
α helix	β turn III
π helix	β turn III
3_{10} helix	β turn III
β sheet	δ turn
De Santis	Not secondary

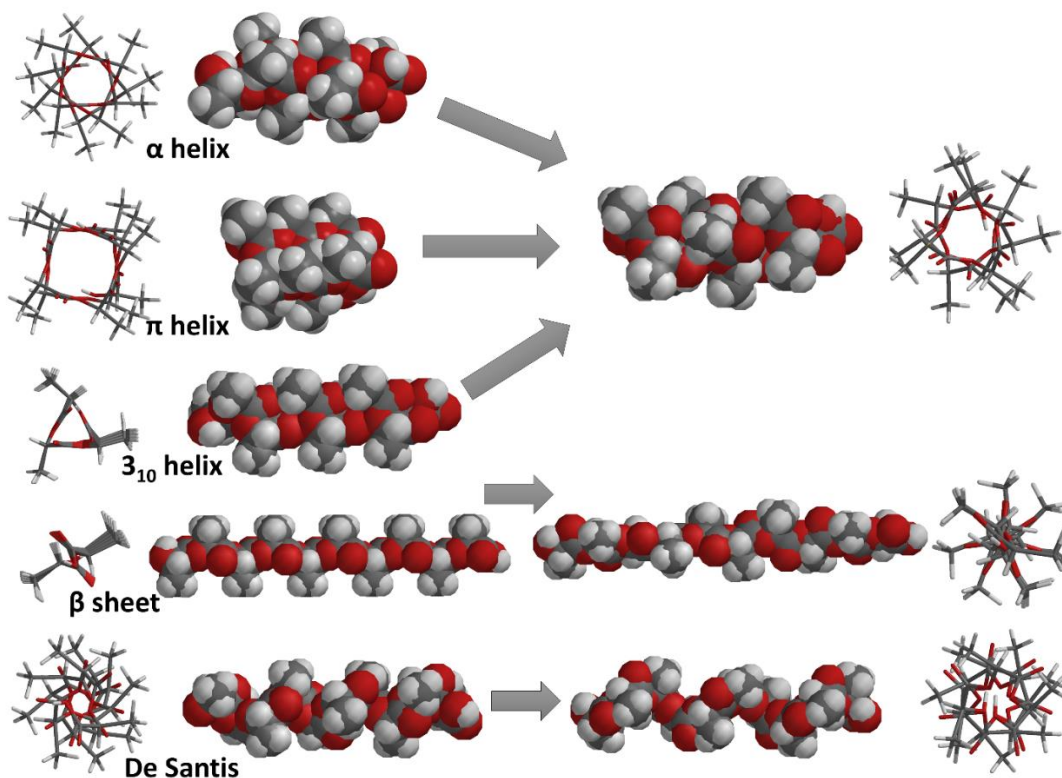


Figure 3. 1. Graphical representations of the canonical PLA structures (left) and of the DFT-optimized geometries obtained starting from these structures. See also Table 3. 2. for numerical details.

The question has been asked, whether in terms of spatial organization for secondary-type structure, polylactic acid (PLA) may be regarded as an analogue of a poly-alanine oligo/polypeptide, where the amino group has been replaced by a hydroxyl. A series of studies have explored the possibility that PLA can adopt peptide-type secondary structures – i.e., repetitive structural patterns characterized by intramolecular hydrogen bonds between neighbouring functional groups. To this end, a range of computational techniques have been applied, looking at relative stabilities of helices (α , π , 3_{10}), and β sheets, as well as at a PLA-specific structure proposed by De Santis. These previous studies have examined the relative energies, general structural features and spectroscopic data of such proposed secondary structure elements of PLA. However, while they did note that the computed (geometry-optimized) structures strayed from the initial canonical shape in terms of overall length, they neglected to describe the state of the Φ and Ψ angles after geometry optimization. Reviewing these data with focus on the higher-quality computational method (the M062x functional, parameterized especially for describing non-covalent interactions – which are the key to describing secondary structure elements), we find that the optimized PLA geometries in fact stray far from the initial Φ , Ψ values – to the extent that all of the peptide-like secondary

structures in fact end up as turns (mostly type III β turns – with a δ turn also possible, but disfavoured energetically), while the DFT-optimized De Santis structure has no classical correspondent in the Ramachandran series of secondary structures. Thus, within the limits of the computational methods employed so far, only two types of spatial organization are proposed as feasible in PLA: peptide-like type III β turns, and a PLA-specific arrangement (based on the structure proposed by De Santis from experimental data) that has no parallel in classical peptide secondary structures. Unlike in peptide secondary structures, the driving force for repetitive three-dimensional structural organization in PLA is not hydrogen bonding between backbone functional groups, but rather steric repulsions and the weak hydrogen bonding between side-chain CH_3 protons and backbone oxygen atoms.

4. Computational contributions to understanding the removal and degradation of sodium diclofenac via radical-based mechanism using *S. sclerotiorum* laccase³

Diclofenac ([2-(2,6-Dichloroanilino)phenyl]acetic acid, typically sold in formulations as sodium, potassium or ammonium salt) is one of the most commonly used nonsteroidal anti-inflammatory drug (NSAID), with analgesic, antipyretic and anti-inflammatory activity.⁵⁴ The half-life of diclofenac sodium in human plasma varies from 1 to 3 hours with a peak plasma concentration that occurs in about 3 hours.⁵⁶ Due to its wide use, diclofenac is one of the most commonly detected compounds in sewage treatment plant effluents and in surface waters. Prolonged exposure to environmentally-relevant concentrations of diclofenac leads to an impairment of the general health condition in fish.^{59–61} Due to its multimodal mechanism of action and ability to penetrate placenta, diclofenac is known to have a range of undesirable side effects.^{62,63}

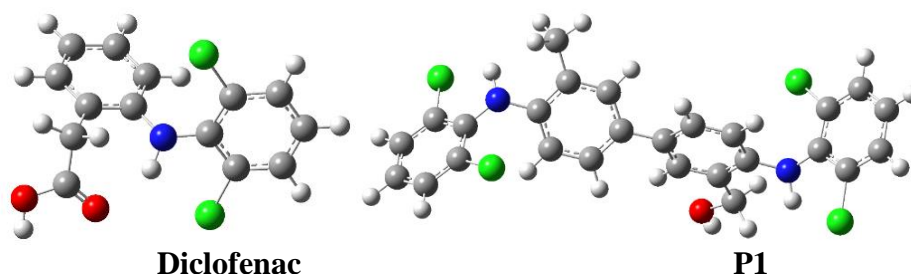
Laccase is a copper-containing oxidoreductase that catalyzes monoelectronic oxidation of various substrates, such as phenols, and aromatic or aliphatic amines, to the corresponding radicals, using molecular oxygen as the final electron acceptor.⁶⁴ Laccases occur widely in fungi; they have been characterized less frequently in higher plants.⁶⁴ Recent reports on the occurrence of laccase and its functions in physiological development and

³ Published as Coman, Cristina and Hadade, Niculina and Pesek, Szilard and Silaghi-Dumitrescu, Radu and Moț, Augustin, Removal and Degradation of Sodium Diclofenac Via Radical-Based Mechanisms Using *S. Sclerotiorum* Laccase. Preprint available as <http://dx.doi.org/10.2139/ssrn.4505088>

industrial utility have shown that this enzyme is able to oxidize various substrates with concomitant uptake of oxygen, depending on molecular weights, pH of medium, and substrate specificity.⁶⁴⁻⁶⁸ We have previously characterized in detail a laccase from *Sclerotinia sclerotiorum* with very good thermal stability and whose remarkable substrate adaptability includes modulation of the active site by covalent modification during the catalytic cycle.⁶⁷⁻⁶⁹

A very wide variety of proposed bioremediation processes on industrial effluents employ laccase. Research in recent years has been intense, much of it being focused on utility of the wide diversity of laccases, or on identification of resulted compounds from their interesting enzymology.^{70,71,80-89,72,90-93,73-79} The current chapter contributes to an ongoing experimental report to investigate the potential of the *S. sclerotiorum* laccase in decomposing a largely used pharmaceutical compound, namely diclofenac, and to identify the by-products resulted from this process with the aid of HPLC coupled with mass-spectrometry and UV-vis detectors. The laccase reaction could be an alternative to some other solutions applied to remove pharmaceutical compounds as emerging pollutants from residual water, such as for example, photocatalytic,⁹⁴ ozonation,^{95,96} or by non-thermal plasma treatment.^{97,98} Specific to the present study is the use of a particularly versatile laccase, a detailed chemical analysis of the products and of the reaction mechanisms, and the advantage of transforming diclofenac into non-soluble material which can be more easily removed from industrial effluents – by contrasts with protocols that simply transform diclofenac into other water-soluble products that still may be biologically active.

Based on the HPLC retention factors (which would be expected to correlate with hydrophobicity) and mass spectra in the HPLC-MS data, structures were proposed for 7 of the products as indicated in Figure 4. 1. The DFT-predicted UV-vis spectra offer a reasonable match to experiment, as shown in Table 4. 1.



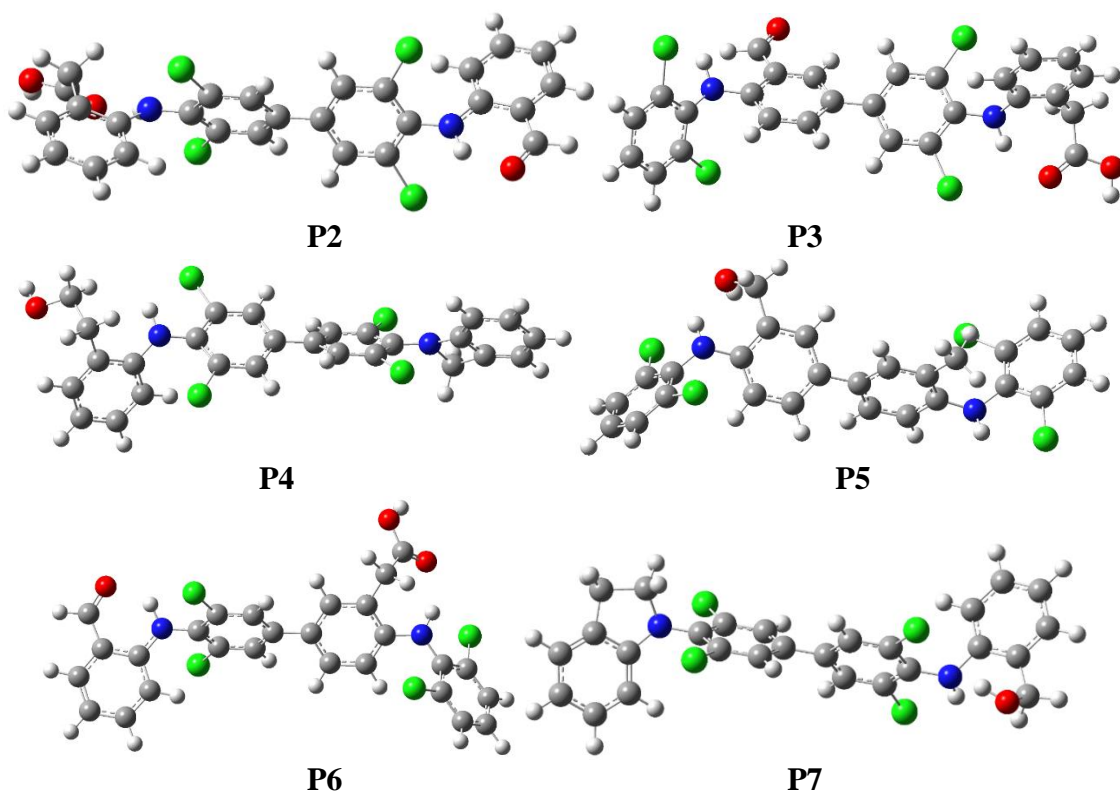


Figure 4. 1. DFT-optimized geometries of diclofenac and of its identified/proposed degradation products.

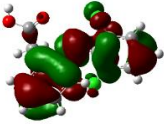
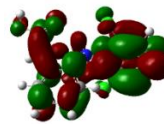
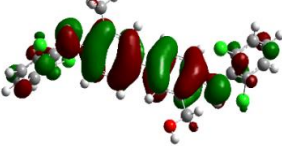
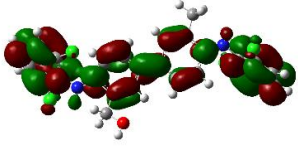
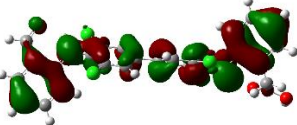
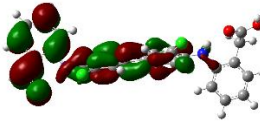
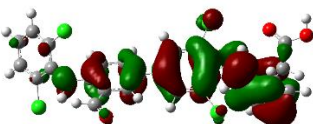
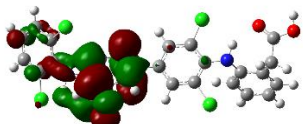
Table 4. 1. Molecular weights (MW, Da), HPLC-MS/UV retention times and UV-vis maxima (see also Figure 10), logP and dipole moments (theoretical, from DFT-optimized geometry), and TD-DFT-predicted UV-vis maxima for diclofenac and for its proposed decomposition products.

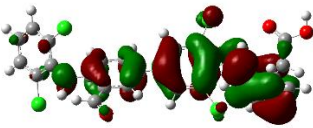

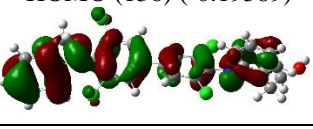
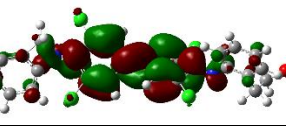
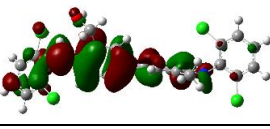
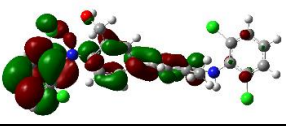
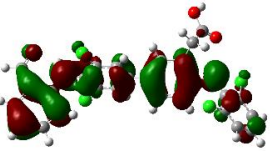
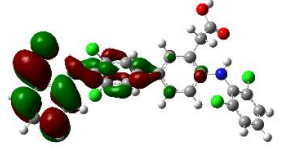
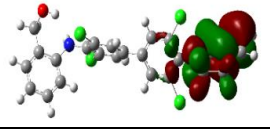
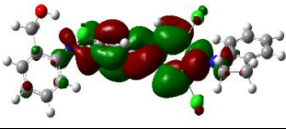
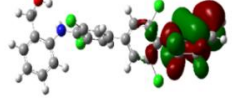
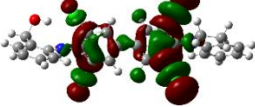
Structure	MW	Retention time (min)	logP	Dipole moment (debye)	UV-vis maxima (nm) (MS)	UV-vis maxima (nm) (TD-DFT)
Diclofenac	295	8.76	3.60	0.41	278	286 (0.26)
P1	516	13.41	7.76	1.18	317	325 (0.90)
P2	558	14.94	7.84	3.91	315 (0.85), 395 (0.06)	361 (0.63)
P3	558	16.17	7.10	4.65	315 (0.85), 395 (0.06)	327 (0.80), 394 (0.09)
P4	514	16.17	7.49	1.60	306 (0.13), 362 (0.03)	361 (0.88)
P5	516	16.79	7.76	0.79	313	303 (0.30)
P6	558	18.78	7.84	3.52	310	358 (0.42)
P7	514	19.06	8.23	2.32	305 (0.57), 384	313 (0.39),

					(0.20)	437 (0.01)
--	--	--	--	--	--------	------------

To conclude, the degradation of sodium diclofenac was assessed using *Sclerotinia sclerotiorum* laccase. Almost complete diclofenac removal (>96%) occurred after 30 h when the drug was added in a defined liquid medium. The mechanism and products were explored with experimental techniques complemented by TD-DFT calculations. The use of *S. sclerotiorum* laccase in order to eliminate diclofenac proved to be simple and cheap compared to other methods that can be found in the literature. Moreover, it can be an alternative to those procedures that involve strong oxidizing agents, well known for their disadvantages. This may form the basis for efficient wastewater cleaning protocols.

Table 4. 2. Wavelengths (λ , nm), oscillator strengths (OS), and key orbitals closest to the visible region of the UV-vis spectra of diclofenac and its products.

Model	λ	OS	Orbitals responsible (energies indicated in eV)	
diclofenac	286	0.2622	HOMO (76) (-0.20412) 	LUMO (77) (-0.02241) 
P1	325	0.9015	HOMO (133) (-0.18640) 	LUMO (134) (-0.02799) 
P2	361	0.6304	HOMO (143) (-0.20570) 	LUMO (144) (-0.06207) 
P3	394	0.0939	HOMO (143) (-0.19962) 	LUMO (144) (-0.06813) 
	327	0.7954	HOMO (143) (-0.32238)	LUMO +1 (145) (-0.04278)

				
P4	361	0.8769	HOMO (136) (-0.19589) 	LUMO (137) (-0.05317) 
P5	303	0.3042	HOMO (133) (-0.20166) 	LUMO (134) (-0.02777) 
P6	358	0.4204	HOMO (143) (-0.20376) 	LUMO (144) (-0.05833) 
P7	437	0.0024	HOMO (136) (-0.18831) 	LUMO (137) (-0.05950) 
	313	0.3858	HOMO (136) (-0.18831) 	LUMO +5 (142) (-0.01650) 

5. Prediction of UV-vis and fluorescence properties in a series of phenathiazonium derivatives

Phenathiazonium is a type of compound that belongs to the phenothiazine family. It is characterized by a phenothiazine ring structure with an additional quaternary ammonium group attached. This quaternary ammonium group makes phenathiazonium a positively charged molecule. By introducing substituents such as N-alkyl chains and/or (hetero)aromatic rings, changes in the pharmaceutical properties of these substances have been found, showing properties antiviral, antimicrobial, anti-inflammatory, antioxidant or even antitumor.⁹⁹ A representative member of this class of substances is methylene blue, which is a cationic dye derived from phenothiazine (3,7-bis(dimethylamino)phenothiazine-5-ium). Featuring useful photophysical, electrochemical or biological properties, methylene blue can also be considered as a model compound for analogues that have substituents attached to the carbon atoms of the peripheral aromatic rings.¹⁰⁰ Such derivatives have also been used as dyes and

stains in biological research. Additionally, some phenathiazonium derivatives have shown potential as photosensitizers in photodynamic therapy, a treatment modality for certain types of cancer.¹⁰¹

In this work, we wanted to study how side substituents can be used to modify the absorption and fluorescence maxima to move them to higher wavelengths towards the near infrared (NIR) range, in the context where our experimentalist collaborators are trying to design methylene blue derivatives/analogues with application as imaging tools for surgery, or as therapeutic agents, or both (theranostics).

Two classes of compounds are examined in the present study: one entailing aliphatic substituents to the central aromatic phenazathionium unit (Figure 5.2).

For the aliphatic class, as seen in

Table 5. 1., in vacuum all investigated compounds show a maximum above 500 nm, with very small differences between models, in the order F1 (514 nm) > 4 > 1 > 3 > 2 ~ F2 > F3 (503 nm). From the point of view of the intensity of the maxima, the compounds present values very close to each other – with a difference of 25% between the extremes of the values; the order of magnitude is 3 > 4 > F3 > 1 > 2 > F2 > F1. The TD-DFT method used here underestimates the wavelength relative to the experimental data, but is reasonably accurate with respect to qualitative elements (eg, differences, order of magnitude). In the present case, one can note the extremely small difference between the compounds both in terms of peak intensity and wavelengths. Such differences are at the accuracy limit of DFT methods.

The effect of the solvent on the maxima in the visible range of the compounds is notable in relation to the vacuum system - a bathochromic shift of about 30 nm in all cases. The differences between the solvents are only at most 3 nm, in the order DMSO > ethanol > water. The solvent also brings about an increase in the intensity of the maxima, of ~20% for the series 1–4 and somewhat less (up to only 13% for F1) in the series F1–F3. The highest increase is provided by DMSO (22-24%) and the lowest by water (19-20%).

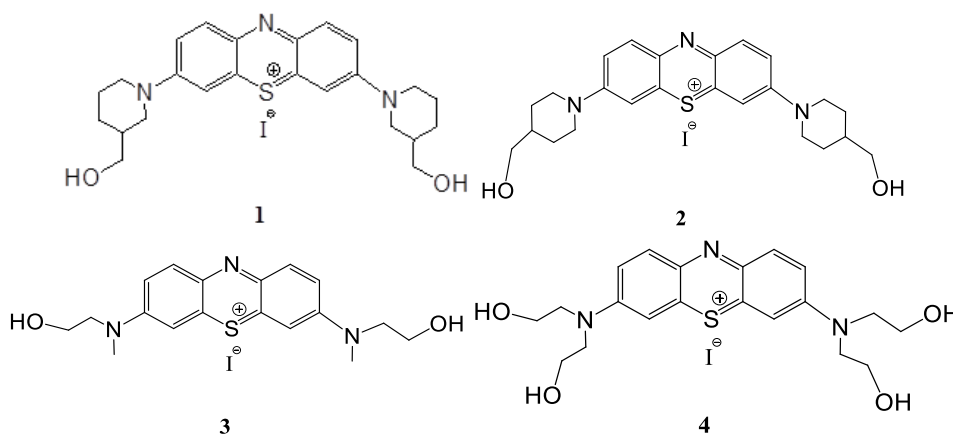
Table 5. 1. also allows tracing the nature of the maximum in the visible range for the studied compounds. It is generally a HOMO-LUMO transition, where the two orbitals have clearly different localizations, so it is a charge transfer band (as can also be deduced from the value of the extinction coefficient / oscillator strength, also typical for such bands). The HOMO is located predominantly on the sulfur atom and those close to it – up to the nitrogen atoms of the amine side substituents; for systems 3 and 4, these side substituents present

heteroatoms sufficiently close to the nitrogen to also contribute to the HOMO, which may explain why 3 and 4 exhibit the longest wavelengths in the series. The LUMO orbital also retains the sulfur component, but is now centered on the rest of the phenazionic system – namely the atoms that did not contribute to the HOMO (including nitrogen). The charge transfer nature of this maximum may also explain the notable solvent effect.

As seen in

Table 5. 1., in the case of model 1 and model 2, where the $-CH_2-OH$ group is in position 3 and 4, respectively, the charge transfer takes place between the HOMO orbital (113) and the LUMO orbital (114), even when using solvents. In vacuum we have the wavelength at 511 nm, but using solvent we reach around 540 nm. The same can be observed in the case of models 2, 3 and 4: in vacuum we have a wavelength at 505 nm, 509 nm and 513 nm respectively, but in solvents the wavelength changes and rises to around 540 nm. The electron excitation in model 3 is from HOMO (91) to LUMO (92), while in model 4 it is from HOMO (107) to LUMO (108).

For models F1, F2, F3 and F4, the wavelength in vacuum is between 503 nm and 514 nm, in solvent (water) rising to wavelengths between 531 nm and 541 nm. For F1 in vacuum, the excitation is from HOMO -2 (220) to LUMO (224), while in water from HOMO (223) to LUMO (224). For F2 in vacuum, the excitation is from HOMO -5 (218) to LUMO (224), while in water it is from HOMO -1 (222) to LUMO (224). In the case of the F3 model, in vacuum the charge transfer is from HOMO -7 (194) to LUMO (202), while in water this transfer is from HOMO -1 (200) to LUMO (202). In the F4 model, a jump from HOMO -6 (211) to LUMO (218) is observed in vacuum, and if we use water as solvent, the excitation is from HOMO -1 (216) to LUMO (218).



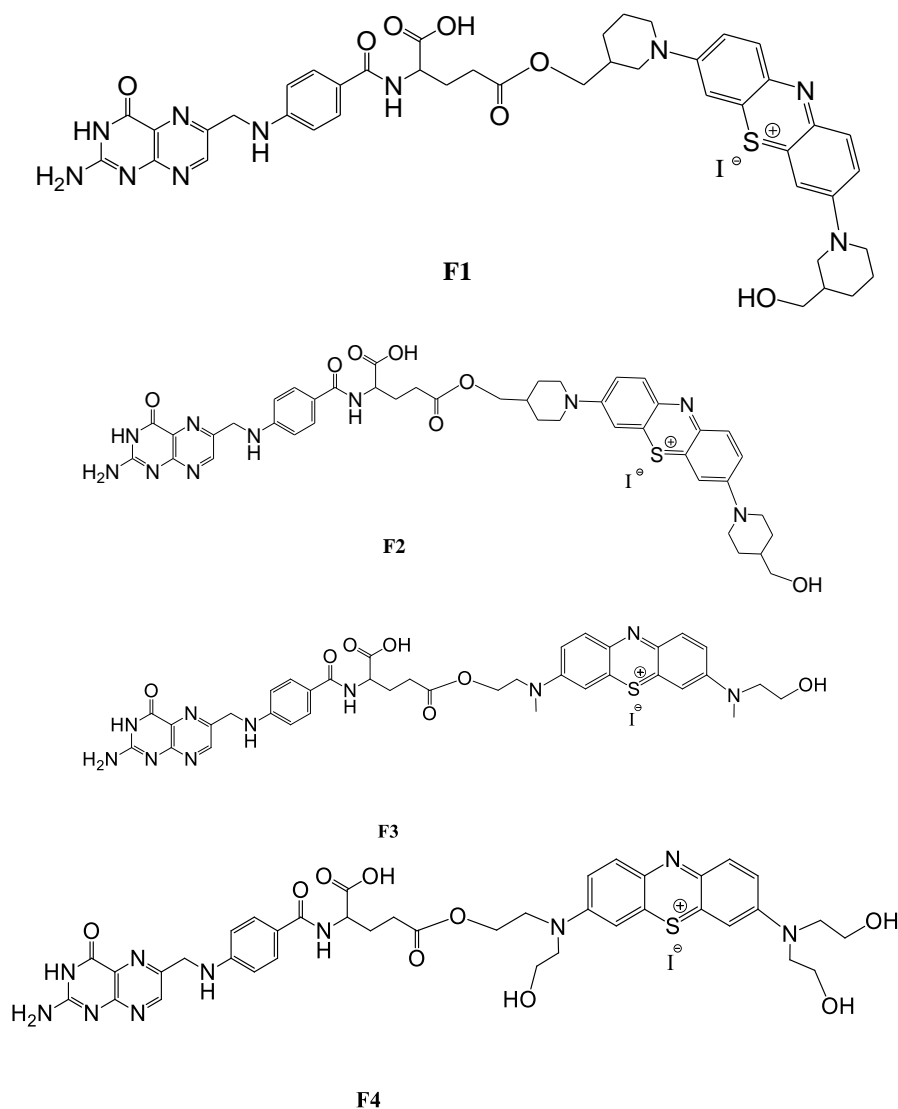
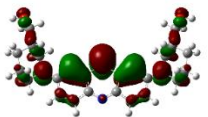
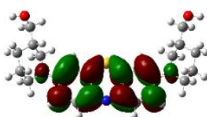
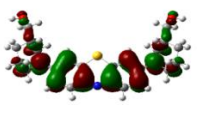
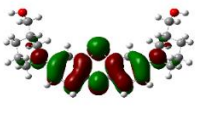
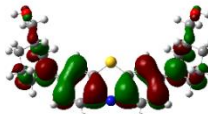
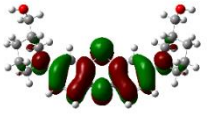
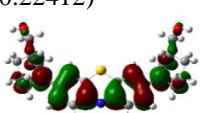
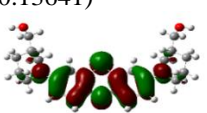




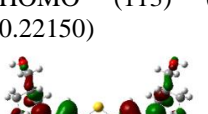
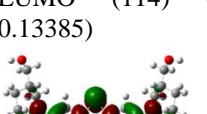


Figure 5. 1. Structures of investigated phenazathionium dyes (1-4) and esters of folic acid with phenazathionium dyes (F1-F4)

Table 5. 1. Key features of the TD-DFT spectra of the investigated compounds.

Model	solvent	Wavelength for the maximum in the visible range	Oscillator strength	Transition	The main responsible orbitals (the number of the orbital for the respective system is presented in parentheses)	
1	vacuum	511	0.9859	HOMO (113) → LUMO (114) 76.44%	HOMO (113) (-0.31473)	LUMO (114) (-0.2258)
				HOMO -1 (112) → LUMO +1 (115)	HOMO -1 (112) (-0.33867)	LUMO +1 (115) (-0.14836)

				11.19%		
				HOMO (113) <- LUMO (114) 12.36%	HOMO (113) (-0.31473) 	LUMO (114) (-0.2258) 
1	DMSO	544	1.2092	HOMO (113) -> LUMO (114) 100%	HOMO (113) (-0.22232) 	LUMO (114) (-0.13465) 
1	ethanol	541	1.1890	HOMO (113) -> LUMO (114) 87.48%	HOMO (113) (-0.22412) 	LUMO (114) (-0.13641) 
				HOMO (113) <- LUMO (114) 12.51%	HOMO (113) (-0.22412) 	LUMO (114) (-0.13641) 
1	H ₂ O	540	1.1783	HOMO (113) -> LUMO (114) 87.35%	HOMO (113) (-0.22150) 	LUMO (114) (-0.13385) 
				HOMO (113) <- LUMO (114) 12.64%	HOMO (113) (-0.22150) 	LUMO (114) (-0.13385) 

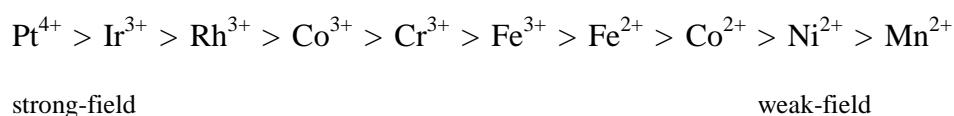
A comprehensive TD-DFT investigation of a series of aliphatic- and aromatic-substituted phenazathionium derivatives of methylene blue is reported in this chapter. The focus is set on the visible and NIR region of the spectrum, with three main issues to follow: (1) the position of absorption maxima, with a focus on identifying the compounds with maxima at longer wavelengths, with higher extinction coefficients (2) excited-state behaviour, either implicitly by employing vertical calculations or explicitly by examining the geometries of excited states, in order to explore the fluorescence potential of the compounds, and (3) the molecular orbital nature of the transitions in this region (especially with the

implication that such knowledge would allow more straightforward / rational design of compounds with better properties cf. the above-discussed items 1 and 2). These data are currently being shared with our experimental collaborators, and a detailed comparison with their data will be presented by them. An overall agreement and predictive usefulness of the calculations were noted in ¹⁰², for which the calculations reported here formed a basis even if the author of this thesis was not nominally an author.

6. DFT evaluation of the spectrochemical series

Based on the results of absorption spectra of Co(III) complexes, in 1938 an arrangement of ligands was proposed, with weak ligands on the left and strong ligands on the right, called the spectrochemical series of ligands¹⁰³. The authors in reference ¹⁰³ used the electronic absorption maxima in the visible region as a proxy, operating with the interpretation that electronic excitation occurs in these bands between the d orbitals – and can then offer a measure of the orbital splitting in terms of Δ or related parameters.

The geometry of the complex, the charge of the ion, the ligands around the metal, and the nature of the metal ion cause the splitting of the d orbitals. If we keep the geometry of the complex and the ligand constant, we see the splitting decrease in the order:



On the left we thus find ions with a weak field, where the division of the crystal field is small, and on the right we find ions with a strong field, where the division of the crystal field is high. If we keep the geometry of the complex and the metal constant, this division has the following form (from small Δ to large Δ ¹⁰⁴): $\text{I}^- < \text{Br}^- < \text{S}^{2-} < \text{SCN}^-$ (S-bonded) $< \text{Cl}^- < \text{NO}_3^- < \text{N}_3^- < \text{F}^- < \text{OH}^- < \text{C}_2\text{O}_4^{2-} < \text{H}_2\text{O} < \text{NCS}^-$ (N-bonded) $< \text{CH}_3\text{CN} < \text{py}$ (pyridine) $< \text{NH}_3 < \text{en}$ (ethylenediamine) $< \text{bipy}$ (2,2'-bipyridine) $< \text{phen}$ (1,10-phenanthroline) $< \text{NO}_2^-$ (N-bonded) $< \text{PPh}_3$ (Triphenylphosphine) $< \text{CN}^- < \text{CO}$.

The spectrochemical series of ligands, as laid out above, is by far not universal. For instance, in ferric heme complexes throughout biology it is generally recognized that fluoride complexes are always high-spin while hydroxide complexes are always low-spin, azide complexes are typically low-spin, and water complexes are generally high-spin although they can sometimes be low-spin (e.g., in cytochrome P450).¹⁰⁵⁻¹⁰⁷ The experimental

data on ferric heme complexes would thus suggest an order of ligand strength with hydroxide weaker than water (in conflict with the spectrochemical series), or azide weaker than fluoride (in conflict with the spectrochemical series). Further conflict would ensue if discussing other heme ligands, such as nitrite or sulfide.^{108–112}

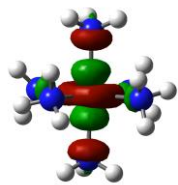
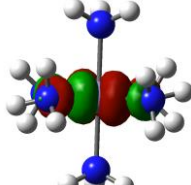
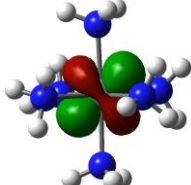
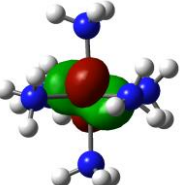
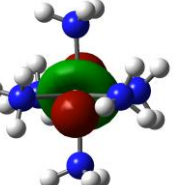
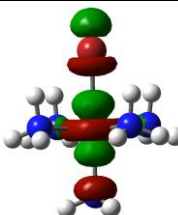
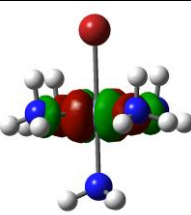
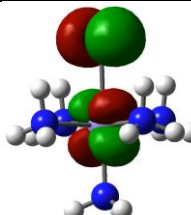
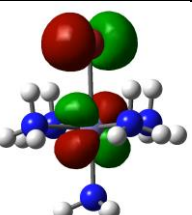
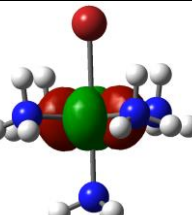
A DFT comparison with the spectrochemical series would logically employ simulation of the UV-vis spectra, to be compared with the original ones from 1938 on the respective series of Co(III) complexes.¹⁰³ Simulations of these spectra on Co models (not reported here) as well as on the iron models reported here using TD-DFT (not shown) revealed, however, no meaningful way to identify a band in the DFT predicted spectrum that would match against the experimental ones. Thus, the TD-DFT spectra featured a multitude of bands, with complex characters, rather than the expected/hoped simple $d \rightarrow d$ transitions wherewith the 1938 experimental data were interpreted. It is important to note that the experimental UV-vis spectra are a proxy rather than a faithful reflection of the strength of the ligands. In a reasonable approximation, the bands seen in the visible region of the electronic absorption spectrum may be considered as due to transitions between the two sets of d orbitals in an octahedral field. However, as also illustrated in the previous chapters, UV-vis spectra can in fact be much more complex. On the other hand, DFT calculations do allow for two more direct methods of assessing the relative strengths of ligands: (1) simply comparing the energy of the low-spin vs. the high-spin state of a series of complexes where one single ligand is replaced in turn by any of the target ligands, and (2) even more straightforwardly, simply comparing the relative energies of the d orbitals in the respective complexes. Therefore, in this section our analysis of the spectrochemical series relies on these two parameters.

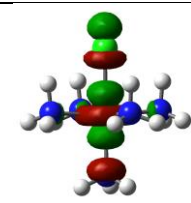
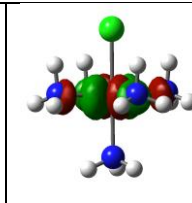
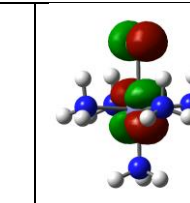
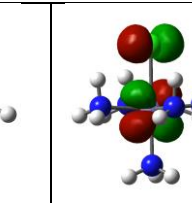
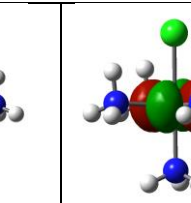
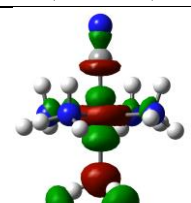
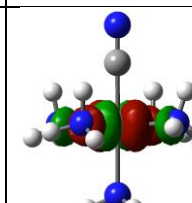
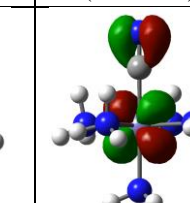
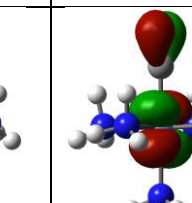
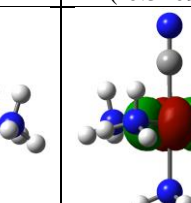
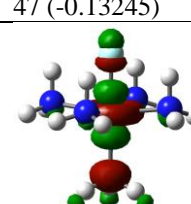
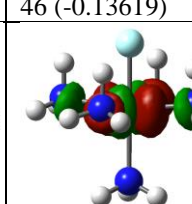
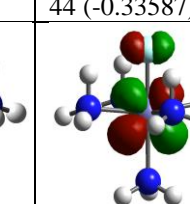
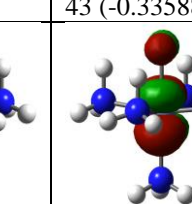
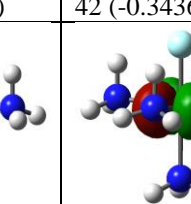
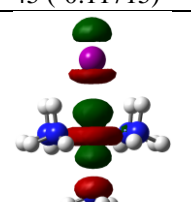
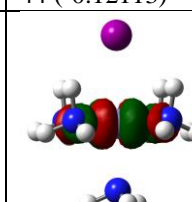
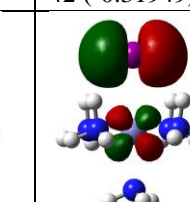
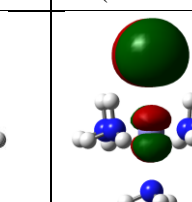
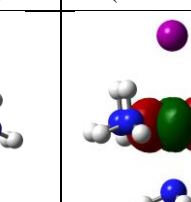
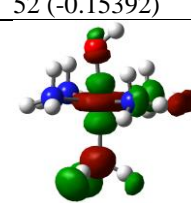
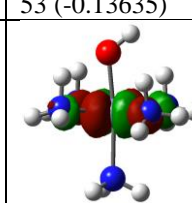
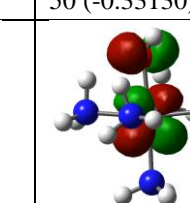
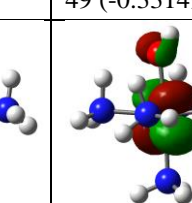
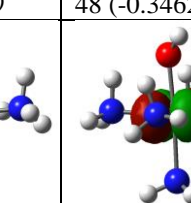
Table 6.1 and Error! Reference source not found.. Show the calculated energies of the high spin and low spin states for Fe(II) and Fe(III) models and the energy difference therefrom (dE), as well as estimations of the Δ parameter. For the latter, since none of the models display perfect octahedral symmetry and hence the t_{2g} and e_g sets of orbitals are not completely degenerate, two versions of the Δ values are proposed. Thus, Δ_a is defined as the difference between the energies of arithmetic average of the energies of the two e_g orbitals and the arithmetic average of the three t_{2g} orbitals. Then, Δ_l is defined as the difference between the lowest-energy e_g orbital and the highest-energy t_{2g} orbital. Table 6. 2. and Error! Reference source not found.. show the molecular orbitals taken into account for these Δ calculations.

Table 6. 1. Absolute and relative energies (kcal/mol) for the Fe(II) structures, ordered by the values predicted by the calculations, top being the strongest ligand and bottom the weakest; $dE = E_{\text{high spin}} - E_{\text{low spin}}$; ($\Delta_a = ((d_{x^2-y^2} + d_{z^2})/2) - ((d_{xz} + d_{yz} + d_{xy})/3)$, $\Delta_l = \min(d_{z^2}, d_{x^2-y^2}) - \max(d_{xz}, d_{yz}, d_{xy})$).

	$E_{\text{high spin}}$	$E_{\text{low spin}}$	dE	Δ_a	Δ_l
$\text{Fe}^{2+}-(\text{NH}_3)_5\text{-CN}^-$	-1028772.96	-1028768.98	-3.99	0.2041433	0.19968
$\text{Fe}^{2+}-(\text{NH}_3)_5\text{-PCH}_3$	-1259700.07	-1259690.37	-9.71	0.2072483	0.20571
$\text{Fe}^{2+}-(\text{NH}_3)_5\text{-CH}_3\text{CN}$	-1053654.03	-1053644.00	-10.03	0.213	0.2109
$\text{Fe}^{2+}-(\text{NH}_3)_5\text{-Py}$	-1125912.55	-1125901.30	-11.25	0.2016633	0.18425
$\text{Fe}^{2+}-(\text{NH}_3)_5\text{-NO}_2^-$	-1099275.50	-1099264.20	-11.30	0.205405	0.20201
$\text{Fe}^{2+}-(\text{NH}_3)_5\text{-NO}_3^-$	-1146480.43	-1146468.26	-12.17	0.20691	0.2024
$\text{Fe}^{2+}-(\text{NH}_3)_5\text{-Br}^-$	-2585829.37	-2585816.83	-12.54	0.19801	0.18925
$\text{Fe}^{2+}-(\text{NH}_3)_5\text{-CH}_3\text{NH}_2$	-1030485.59	-1030472.98	-12.60	0.2092417	0.20852
$\text{Fe}^{2+}-(\text{NH}_3)_6$	-1005813.75	-1005801.06	-12.69	0.2080317	0.20644
$\text{Fe}^{2+}-(\text{NH}_3)_5\text{-SCN}^-$	-1278678.07	-1278664.93	-13.14	0.1960167	0.17705
$\text{Fe}^{2+}-(\text{NH}_3)_5\text{-NCS}^-$	-1278687.80	-1278673.06	-14.73	0.17779	0.1594
$\text{Fe}^{2+}-(\text{NH}_3)_5\text{-Cl}^-$	-1259324.73	-1259309.54	-15.19	0.200485	0.19416
$\text{Fe}^{2+}-(\text{NH}_3)_5\text{-I}^-$	-1157399.17	-1157383.93	-15.24	0.1912183	0.17738
$\text{Fe}^{2+}-(\text{NH}_3)_5\text{-F}^-$	-1033205.29	-1033188.67	-16.62	0.2039433	0.19836
$\text{Fe}^{2+}-(\text{NH}_3)_5\text{-OH}^-$	-1018110.16	-1018092.46	-17.71	0.1994033	0.18932
$\text{Fe}^{2+}-(\text{NH}_3)_5\text{-N}_3^-$	-1073645.08	-1073626.60	-18.48	0.1903467	0.1779
$\text{Fe}^{2+}-(\text{NH}_3)_5\text{-S}^{2-}$	-1220497.49	-1220463.54	-33.94	0.0868067	0.06032

Table 6. 2. Key frontier orbitals and absolute energies (a.u.) from the DFT spectra of the Fe(II) models (numbers of orbitals and absolute energies (a.u.) are shown).

Name	d_z^2	$d_{x^2-y^2}$	d_{xz}	d_{yz}	d_{xy}
$\text{Fe}^{2+}-(\text{NH}_3)_6$	 45 (-0.28484)	 44 (-0.28789)	 42 (-0.49433)	 41 (-0.49435)	 40 (-0.49451)
$\text{Fe}^{2+}-(\text{NH}_3)_5\text{-Br}^-$	 57 (-0.14585)	 58 (-0.13421)	 55 (-0.33510)	 54 (-0.33512)	 53 (-0.34390)

Fe ²⁺ - (NH ₃) ₅ -Cl ⁻					
	48 (-0.13868)	49 (-0.13145)	46 (-0.33284)	45 (-0.33285)	44 (-0.34096)
Fe ²⁺ - (NH ₃) ₅ -CN ⁻					
	47 (-0.13245)	46 (-0.13619)	44 (-0.33587)	43 (-0.33588)	42 (-0.34364)
Fe ²⁺ - (NH ₃) ₅ -F ⁻					
	45 (-0.11715)	44 (-0.12113)	42 (-0.31949)	41 (-0.31949)	40 (-0.33027)
Fe ²⁺ - (NH ₃) ₅ -I ⁻					
	52 (-0.15392)	53 (-0.13635)	50 (-0.33130)	49 (-0.33149)	48 (-0.34627)
Fe ²⁺ - (NH ₃) ₅ -OH ⁻					
	45 (-0.11251)	44 (-0.11529)	42 (-0.30461)	41 (-0.31312)	40 (-0.32218)

In this chapter, the geometries of Fe(II) and Fe(III) compounds were optimized and we measured the energy difference between high spin and low spin and between *d* orbitals and compared it with the experimentally measured spectrochemical series.

The ligands that we find in the spectrochemical series are arranged according to their ability to arrange the *d* orbitals of a metal ion in a complex. This depends on several factors, including the size and charge of the ligand. The calculations reported here reveal some unexpected conclusions: (1) there is very little agreement between the calculations and the experimentally-known spectrochemical series, (2) the series predicted from Fe(II) models differs from the ones predicted for Fe(III) models, and (3) the series predicted based on energy differences between low- and high-spin states of the same complex differ from the series predicted based on *d* orbital energies within the low-spin complexes. These findings

suggest a need for more thorough exploration of the issue, examining other metals (indeed, the Co(III) models are currently pursued in another PhD thesis) and also of the computational approaches (e.g., other functionals, solvation). Such studies are underway at the moment.

7. Conclusions

The present thesis attempts to employ the modern tools of computational chemistry in order to illustrate applications on issues of very general interest, that may be translatable or relatable for pre-college and early-college students. Four topics are chosen for computational exploration.

At the beginning of this thesis, we aimed to find a clarification of the mechanism in the starch-iodine reaction using, in addition to calculations with time-dependent density functional calculations (TD-DFT) and experiments. Starting from the idea that the iodine-iodine distance in the iodine-amylose complex was experimentally proven to be 3.1 Å, using these data in DFT calculations, we concluded that a $I_2-I_5^-$ unit would provide the best fit with experimental data. In this contest, I_2/I_n^- pairs with charge transfer bands from the occupied I_n^- ($n>3$) σ^* to the empty $I_2 \sigma^*$ orbital are considered to be reasonably responsible for the blue color.

In the next chapter, the previous work of PhD student Izabela Irsai related to polylactic acid was expanded upon, having as points of interest the influence of weak intra- and intermolecular interactions on the general shape or conformation of molecules. Previous studies may have less emphasis on describing the state of the Φ and Ψ angles after geometry optimization, so with the help of the M062x functional we concluded that the optimized PLA geometries deviate from the initial values of Φ and Ψ . With the help of the calculations used, two types of PLA organization are proposed, peptide-like type III β towers and a specific arrangement of PLA (based on the structure proposed by De Santis from experimental data) that has no parallels in classical peptide secondary structures.

In the third chapter of original contributions, we use TD-DFT calculations, which complement the data from previous experiments related to diclofenac sodium degradation, performed in the presence of the *Sclerotinia sclerotiorum* laccase. The collected data showed that the elimination of diclofenac can be achieved in a simple, fast and cheap way.

The fourth chapter follows TD-DFT calculations to predict color and fluorescence variations between a range of organic compounds such as aliphatic and aromatic substituted

phenazathionium derivatives of methylene blue. The position of the absorption maxima, the behavior in the excited state, and the molecular orbital nature of the transitions in this region were considered and analyzed.

The fifth chapter enters the world of transition metal chemistry, following an analysis of the spectrochemical series using DFT calculations and molecular orbital analysis. After optimizing the geometries of Fe(II) and Fe(III) compounds, the energy difference between high spin and low spin and between d orbitals was calculated and compared with the experimentally measured spectrochemical series. Based on the collected data, we can conclude that the experimentally known spectrochemical series and the spectrochemical series proposed by means of calculations are in very little agreement with each other. Using these conclusions, further studies and computational approaches are proposed.

References

- (1) Nelson; David; Michael M. Cox. Principles of Biochemistry. *Principles of Biochemistry*; W.H. Freeman and Company: New York, 2008; Vol. 5th ed.
- (2) Green, M. M.; Blankenhorn, G.; Hart, H. Which Starch Fraction Is Water-Soluble, Amylose or Amylopectin? *J. Chem. Educ.* **1975**, *52* (11), 729. <https://doi.org/10.1021/ed052p729>.
- (3) Katz, J. R. Abhandlungen Zur Physikalischen Chemie Der Stärke Und Der Brotbereitung. *Zeitschrift für Phys. Chemie* **1930**, *150A* (1), 37–59. <https://doi.org/10.1515/zpch-1930-15005>.
- (4) Katz, J. R.; Derksen, J. C. Abhandlungen Zur Physikalischen Chemie Der Stärke Und Der Brotbereitung. *Zeitschrift für Phys. Chemie* **1933**, *167A* (1), 129–136. <https://doi.org/10.1515/zpch-1933-16714>.
- (5) Bear, R. S. The Significance of the “V” X-Ray Diffraction Patterns of Starches ¹. *J. Am. Chem. Soc.* **1942**, *64* (6), 1388–1392. <https://doi.org/10.1021/ja01258a043>.
- (6) Meyer, K. H.; Bernfeld, P.; Wolf, E. Recherches Sur l’amydon III. Fractionnement et Purification de l’amylose de Maïs Naturel. *Helv. Chim. Acta* **1940**, *23* (1), 854–864. <https://doi.org/10.1002/hlca.194002301110>.
- (7) Sarko A; Zugenmaier P. Fiber Diffraction Methods. *Am. Chem. Soc. Washingt. DC* **1980**, *141*, 459–482.
- (8) Rappenecker G.; Zugenmaier P. *Carbohydr Res.* **1981**, *89*, 11–19.
- (9) Murphy V.G.; Zaslow B.; French A.D. *Biopolymers.* **1975**, *14*, 1487–1501.
- (10) Brisson J.; Chanzy H.; Winter W.T. *Int J Biol Macromol.* **1991**, *13*, 31–39.
- (11) Veregin R.P.; Fyfe C.A.; Marchessault R.H. *Macromolecules.* **1987**, *20*, 3007–3012.
- (12) Gidley M.J.; Bociek S.M. *J Am Chem Soc.* **1988**, *110*, 3820–3829.
- (13) Imberty, A.; Chanzy, H.; Pérez, S.; Bulèon, A.; Tran, V. The Double-Helical Nature of the Crystalline Part of A-Starch. *J. Mol. Biol.* **1988**, *201* (2), 365–378. [https://doi.org/10.1016/0022-2836\(88\)90144-1](https://doi.org/10.1016/0022-2836(88)90144-1).
- (14) Saenger W. *Inclusion Compounds*; Atwood, J. L., Davies, J. E. D., MacNicol, D. D., Eds.; Academic: London, 1984; Vol. 2.
- (15) Harata, K. *Comprehensive Supramolecular Chemistry*; Atwood, J. L., Davies, J. E. D., MacNicol, D. D., Eds.; Pergamon: Oxford, 1996; Vol. 3.
- (16) J. Brisson; H. Chanzy; W.T. Winter. The Crystal and Molecular Structure of Vh Amylose by Electron Diffraction Analysis. *Int. J. Biol. Macromol.* **1991**, *13*, 31–39.
- (17) Cohen, R.; Orlova, Y.; Kovalev, V.; Ungar, Y.; Shimoni, E. Structural and Functional Properties of Amylose Complexes with Genistein. *J. Agric. Food Chem.* *56(11)*, 4212–4218.
- (18) Sarko, A.; Wu, H.-C. . The Crystal Structures of A-, B- and C-Polymorphs of Amylose and Starch. *Starch-Starke* **1978**, *30(3)*, 7378.

- (19) Rani, A.; Ali, U. Degree-Based Topological Indices of Polysaccharides: Amylose and Blue Starch-Iodine Complex. *J. Chem.* **2021**, *2021*, 1–10. <https://doi.org/10.1155/2021/6652014>.
- (20) Landolt, H. Uber Die Zeitdauer Der Reaction Zwischen Jodsaure Und Schwefliger Saure. *Ber. Dtsch. Chem. Ges.* **1886**, *19*, 1317–1365.
- (21) Gilbert, G. A.; Marriott, J. V. R. Starch-Iodine Complexes. Part I. *Trans. Faraday Soc.* **1948**, *44*, 84. <https://doi.org/10.1039/tf9484400084>.
- (22) Stein, R. S.; Rundle, R. E. On the Nature of the Interaction between Starch and Iodine. *J. Chem. Phys.* **1948**, *16* (3), 195–207. <https://doi.org/10.1063/1.1746834>.
- (23) Thoma, J. A.; French, D. The Starch-Iodine-Iodide Interaction. Part I. Spectrophotometric Investigations ¹. *J. Am. Chem. Soc.* **1960**, *82* (16), 4144–4147. <https://doi.org/10.1021/ja01501a004>.
- (24) Nishimura, T.; Yajima, H.; Kubota, S.; Ishii, T.; Endo, R. Polymer Effect on the Iodine Coloring Species Responsible for the Spectroscopic Properties of Amylose-Iodine Complexes. *Kobunshi Ronbunshu* **1990**, *47* (9), 717–725. <https://doi.org/10.1295/koron.47.717>.
- (25) Hiromi, K.; Shibaoka, T.; Ono, S. Kinetic Studies of Amylose-Iodine-Iodide Reaction by Stopped-Flow Method*. *J. Biochem.* **1970**, *68* (2), 205–214. <https://doi.org/10.1093/oxfordjournals.jbchem.a129348>.
- (26) Yajima, H.; Nishimura, T.; Ishii, T.; Handa, T. Effect of Concentration of Iodide on the Bound Species of I₂/I⁻3 in the Amylose-Iodine Complex. *Carbohydr. Res.* **1987**, *163* (2), 155–167. [https://doi.org/10.1016/0008-6215\(87\)80179-9](https://doi.org/10.1016/0008-6215(87)80179-9).
- (27) Cronan, C. L.; Schneider, F. W. Cooperativity and Composition of the Linear Amylose-Iodine-Iodide Complex. *J. Phys. Chem.* **1969**, *73* (11), 3990–4004. <https://doi.org/10.1021/j100845a073>.
- (28) Cramer, F.; Herbst, W. Die Lichtabsorption von Jodkettenmolekeln. *Naturwissenschaften* **1952**, *39* (11), 256–256. <https://doi.org/10.1007/BF00630876>.
- (29) Bersohn, R.; Isenberg, I. Metallic Nature of the Starch-Iodine Complex. *J. Chem. Phys.* **1961**, *35* (5), 1640–1643. <https://doi.org/10.1063/1.1732123>.
- (30) Rundle, R. E. The Configuration of Starch and Starch-Iodine Complex. I. The Dichroism of Flow of Starch-Iodine Solutions. *J. Am. Chem. Soc.* **1943**, *65*, 554–558.
- (31) Rundle, R. E. The Configuration of Starch in the Starch-Iodine Complex. V. Fourier Projections from X-Ray Diagrams. *J. Am. Chem. Soc.* **1947**, *69*, 1769–1772.
- (32) Noltemeyer, M.; Saenger, W. X-Ray Studies of Linear Polyiodide Chains in α -Cyclodextrin Channels and a Model for the Starch-Iodine Complex. *Nature* **1976**, *259* (5545), 629–632. <https://doi.org/10.1038/259629a0>.
- (33) Bluhm, T. L.; Zugenmaier, P. Detailed Structure of the Vh-Amylose-Iodine Complex: A Linear Polyiodide Chain. *Carbohydr. Res.* **1981**, *89*, 1–10.
- (34) Handa, T.; Yajima, H. Conformation of Amylose-Iodine-Iodide Complex in Aqueous Solution. *Biopolymers* **1981**, *20* (10), 2051–2072. <https://doi.org/10.1002/bip.1981.360201003>.
- (35) Swanson, A. M. IV. Relation of the Iodine Color to the Structure. *Stud. Struct. polysaccharides* **1947**, 825–837.
- (36) Swanson, M. A. Studies on the Structure of Polysaccharides. IV. Relation of the Iodine Color

- to the Structure. *J. Biol. Chem.* **1948**, *172* (2), 825–837.
- (37) Banks, W.; Greenwood, C. T.; Khan, K. M. The Properties of Synthetic Amylopectin with Long External-Chains. *Starch - Stärke* **1970**, *22* (9), 292–296. <https://doi.org/10.1002/star.19700220903>.
- (38) Hirai, M.; Hirai, T.; Ueki, T. Effect of Branching of Amylopectin on Complexation with Iodine as Steric Hindrance. *Polymer (Guildf)*. **1994**, *35* (10), 2222–2225. [https://doi.org/10.1016/0032-3861\(94\)90255-0](https://doi.org/10.1016/0032-3861(94)90255-0).
- (39) Mould, D. L.; Synge, R. M. Separations of Polysaccharides Related to Starch by Electrokinetic Ultrafiltration in Collodion Membranes. *Biochem. J.* **1954**, *58.4*, 571–600.
- (40) Ono, S.; Tsuchihashi, S.; Kuge, T. On the Starch-Iodine Complex. *J. Am. Chem. Soc.* **1953**, *75*, 3601–3602.
- (41) Nishimura, T.; Yajima, H.; Kubota, S.; Ishii, T.; Endo, R. Effect of I- Concentration on the Optical Properties of Amylose-Iodine Complexes. *Kobunshi Ronbunshu* **1988**, *45* (12), 945–952. <https://doi.org/10.1295/koron.45.945>.
- (42) Agafonov, A. V.; Vladimirov, A. V.; Volkova, T. V. The Concentration Dependences of the Stability Constants of Iodine-Iodide-Amylose Complexes in Aqueous Solutions of Electrolytes. *Russ. J. Phys. Chem. A* **2004**, *78* (9), 1584–1587.
- (43) NISHIMURA, T.; YAJIMA, H.; ISHII, T.; ENDO, R. Effect of Molecular Weight of Amylose on the Iodine Coloring Species Responsible for the Optical Properties of Amylose-Iodine Complexes. *KOBUNSHI RONBUNSHU* **1989**, *46* (9), 537–544. <https://doi.org/10.1295/koron.46.537>.
- (44) Dintzis, F. R.; Tobin, R.; Beckwith, A. C. Amylose-Iodine Complex. II. Molecular Weight Estimates. *Macromolecules* **1976**, *9* (3), 478–482. <https://doi.org/10.1021/ma60051a018>.
- (45) Calabrese, V. T.; Khan, A. Amylose-Iodine Complex Formation without KI: Evidence for Absence of Iodide Ions within the Complex. *J. Polym. Sci. Part A Polym. Chem.* **1999**, *37* (15), 2711–2717. [https://doi.org/10.1002/\(SICI\)1099-0518\(19990801\)37:15<2711::AID-POLA4>3.0.CO;2-6](https://doi.org/10.1002/(SICI)1099-0518(19990801)37:15<2711::AID-POLA4>3.0.CO;2-6).
- (46) Varadarajan, S.; Miller, D. J. Catalytic Upgrading of Fermentation-Derived Organic Acids. *Biotechnol. Prog.* **1999**, *15* (5), 845–854. <https://doi.org/10.1021/bp9900965>.
- (47) Abdel-Rahman, M. A.; Tashiro, Y.; Zendo, T.; Sonomoto, K. Improved Lactic Acid Productivity by an Open Repeated Batch Fermentation System Using *Enterococcus Mundtii* QU 25. *RSC Adv.* **2013**, *3* (22), 8437. <https://doi.org/10.1039/c3ra00078h>.
- (48) Abdel-Rahman, M. A.; Tashiro, Y.; Sonomoto, K. Lactic Acid Production from Lignocellulose-Derived Sugars Using Lactic Acid Bacteria: Overview and Limits. *J. Biotechnol.* **2011**, *156* (4), 286–301. <https://doi.org/10.1016/j.jbiotec.2011.06.017>.
- (49) Li, G.; Zhao, M.; Xu, F.; Yang, B.; Li, X.; Meng, X.; Teng, L.; Sun, F.; Li, Y. Synthesis and Biological Application of Polylactic Acid. *Molecules* **2020**, *25* (21), 5023. <https://doi.org/10.3390/molecules25215023>.
- (50) Irsai, I.; Majdik, C.; Lupan, A.; Silaghi-Dumitrescu, R. Secondary Structure Elements in Polylactic Acid Models. *J. Math. Chem.* **2012**, *50* (4), 703–733.
- (51) Irsai, I.; Lupan, A.; Majdik, C.; Silaghi-Dumitrescu, R. Computational Investigation of Spectroscopic Parameters in Putative Secondary Structure Elements for Polylactic Acid and Comparison with Experiment. *Stud. Univ. Babeş-Bolyai Chem.* **2017**, *62* (4), 495–513.

<https://doi.org/10.24193/subbchem.2017.4.42>.

- (52) Irsai, I.; Brânzanic, A. M. V.; Silaghi-Dumitrescu, R. Polylactic Acid Interactions with Bioceramic Surfaces. *Stud. Univ. Babeş-Bolyai Chem.* **2021**, *66* (3), 107–121. <https://doi.org/10.24193/subbchem.2021.3.06>.
- (53) Irsai, I.; Pesek, S. Z.; Silaghi-Dumitrescu, R. POLYLACTIC ACID INTER-CHAIN INTERACTIONS. *Stud. Univ. Babeş-Bolyai, Chem.* **2022**, *67* (4), 47–72.
- (54) Scholer, D. W.; Ku, E. C.; Boettcher, I.; Schweizer, A. Pharmacology of Diclofenac Sodium. *Am. J. Med.* **1986**, *80* (4 SUPPL. 2), 34–38. [https://doi.org/10.1016/0002-9343\(86\)90077-X](https://doi.org/10.1016/0002-9343(86)90077-X).
- (55) Al-Nimer, M. S. M.; Hameed, H. G.; Mahmood, M. M. Antiproliferative Effects of Aspirin and Diclofenac against the Growth of Cancer and Fibroblast Cells: In Vitro Comparative Study. *Saudi Pharm. J.* **2015**, *23* (5), 483–486. <https://doi.org/10.1016/j.jsps.2015.01.002>.
- (56) Yilmaz, B.; Asci, A.; Palabiyik, S. S. HPLC Method for Determination of Diclofenac in Human Plasma and Its Application to a Pharmacokinetic Study in Turkey. *J. Chromatogr. Sci.* **2011**, *49* (6), 422–427. <https://doi.org/10.1093/chrscl/49.6.422>.
- (57) Lauer, B.; Tuschl, G.; Kling, M.; Mueller, S. O. Species-Specific Toxicity of Diclofenac and Troglitazone in Primary Human and Rat Hepatocytes. *Chem. Biol. Interact.* **2009**, *179* (1), 17–24. <https://doi.org/10.1016/j.cbi.2008.10.031>.
- (58) Zi, J.; Liu, D.; Ma, P.; Huang, H.; Zhu, J.; Wei, D.; Yang, J.; Chen, C. Effects of CYP2C9*3 and CYP2C9*13 on Diclofenac Metabolism and Inhibition-Based Drug-Drug Interactions. *Drug Metab. Pharmacokinet.* **2010**, *25* (4), 343–350. <https://doi.org/10.2133/dmpk.DMPK-10-RG-009>.
- (59) Schwaiger, J.; Ferling, H.; Mallow, U.; Wintermayr, H.; Negele, R. D. Toxic Effects of the Non-Steroidal Anti-Inflammatory Drug Diclofenac. Part I: Histopathological Alterations and Bioaccumulation in Rainbow Trout. *Aquat. Toxicol.* **2004**, *68* (2), 141–150. <https://doi.org/10.1016/j.aquatox.2004.03.014>.
- (60) Saravanan, M.; Hur, J. H.; Arul, N.; Ramesh, M. Toxicological Effects of Clofibric Acid and Diclofenac on Plasma Thyroid Hormones of an Indian Major Carp, *Cirrhinus Mrigala* during Short and Long-Term Exposures. *Environ. Toxicol. Pharmacol.* **2014**, *38* (3), 948–958. <https://doi.org/10.1016/j.etap.2014.10.013>.
- (61) Gröner, F.; Ziková, A.; Kloas, W. Effects of the Pharmaceuticals Diclofenac and Metoprolol on Gene Expression Levels of Enzymes of Biotransformation, Excretion Pathways and Estrogenicity in Primary Hepatocytes of Nile Tilapia (*Oreochromis Niloticus*). *Comp. Biochem. Physiol. Part - C Toxicol. Pharmacol.* **2015**, *167*, 51–57. <https://doi.org/10.1016/j.cbpc.2014.09.003>.
- (62) Chae, J. P.; Park, M. S.; Hwang, Y. S.; Min, B. H.; Kim, S. H.; Lee, H. S.; Park, M. J. Evaluation of Developmental Toxicity and Teratogenicity of Diclofenac Using *Xenopus* Embryos. *Chemosphere* **2015**, *120*, 52–58. <https://doi.org/10.1016/j.chemosphere.2014.05.063>.
- (63) Zloh, M.; Perez-Diaz, N.; Tang, L.; Patel, P.; Mackenzie, L. S. Evidence That Diclofenac and Celecoxib Are Thyroid Hormone Receptor Beta Antagonists. *Life Sci.* **2016**, *146*, 66–72. <https://doi.org/10.1016/j.lfs.2016.01.013>.
- (64) Mot, A. C.; Silaghi-Dumitrescu, R. Laccases: Complex Architectures for One-Electron Oxidations. *Biochem. Biokhimiia* **2012**, *77* (12), 1395–1407. <https://doi.org/Doi10.1134/S0006297912120085>.
- (65) Mayer, A. M.; Staples, R. C. Laccase: New Functions for an Old Enzyme. *Phytochemistry*.

- 2002, pp 551–565. [https://doi.org/10.1016/S0031-9422\(02\)00171-1](https://doi.org/10.1016/S0031-9422(02)00171-1).
- (66) Wang, J.; Feng, J.; Jia, W.; Chang, S.; Li, S.; Li, Y. Lignin Engineering through Laccase Modification: A Promising Field for Energy Plant Improvement. *Biotechnology for Biofuels*. 2015, p 145. <https://doi.org/10.1186/s13068-015-0331-y>.
- (67) Coman, C.; Mot, A. C.; Gal, E.; Parvu, M.; Silaghi-Dumitrescu, R.; Moț, A. C.; Gal, E.; Pârvu, M.; Silaghi-Dumitrescu, R. Laccase Is Upregulated via Stress Pathways in the Phytopathogenic Fungus *Sclerotinia Sclerotiorum*. **2013**, *117* (7–8), 528–539.
- (68) Mot, A. C.; Coman, C.; Hadade, N.; Damian, G.; Silaghi-Dumitrescu, R.; Heering, H. “Yellow” Laccase from *Sclerotinia Sclerotiorum* Is a Blue Laccase That Enhances Its Substrate Affinity by Forming a Reversible Tyrosyl-Product Adduct. *PLoS One* **2020**, *15* (1), : e0225530. <https://doi.org/10.1371/journal.pone.0225530>.
- (69) Mot, A. C.; Pârvu, M.; Damian, G.; Irimie, F. D. D.; Darula, Z.; Medzihradzky, K. F. K. F.; Brem, B.; Silaghi-Dumitrescu, R.; Parvu, M.; Damian, G.; Irimie, F. D. D.; Darula, Z.; Medzihradzky, K. F. K. F.; Brem, B.; Silaghi-Dumitrescu, R.; Moț, A. C.; Pârvu, M.; Damian, G.; Irimie, F. D. D.; Darula, Z.; Medzihradzky, K. F. K. F.; Brem, B.; Silaghi-Dumitrescu, R.; Mot, A. C.; Pârvu, M.; Damian, G.; Irimie, F. D. D.; Darula, Z.; Medzihradzky, K. F. K. F.; Brem, B.; Silaghi-Dumitrescu, R. A “Yellow” Laccase with “Blue” Spectroscopic Features, from *Sclerotinia Sclerotiorum*. *Process Biochem.* **2012**, *47* (6), 968–975. <https://doi.org/DOI 10.1016/j.procbio.2012.03.006>.
- (70) Ihssen, J.; Schubert, M.; Thöny-Meyer, L.; Richter, M. Laccase Catalyzed Synthesis of Iodinated Phenolic Compounds with Antifungal Activity. *PLoS One* **2014**, *9* (3), e89924. <https://doi.org/10.1371/journal.pone.0089924>.
- (71) Palli, L.; Castellet-Rovira, F.; Pérez-Trujillo, M.; Caniani, D.; Sarrà-Adroguer, M.; Gori, R. Preliminary Evaluation of *Pleurotus Ostreatus* for the Removal of Selected Pharmaceuticals from Hospital Wastewater. *Biotechnol. Prog.* **2017**, *33* (6), 1529–1537. <https://doi.org/10.1002/btpr.2520>.
- (72) Lonappan, L.; Rouissi, T.; Laadila, M. A.; Brar, S. K.; Hernandez Galan, L.; Verma, M.; Surampalli, R. Y. Agro-Industrial-Produced Laccase for Degradation of Diclofenac and Identification of Transformation Products. *ACS Sustain. Chem. Eng.* **2017**, *5* (7), 5772–5781. <https://doi.org/10.1021/acssuschemeng.7b00390>.
- (73) Pylypchuk, I. V.; Kessler, V. G.; Seisenbaeva, G. A. Simultaneous Removal of Acetaminophen, Diclofenac, and Cd(II) by *Trametes Versicolor* Laccase Immobilized on Fe₃O₄/SiO₂-DTPA Hybrid Nanocomposites. *ACS Sustain. Chem. Eng.* **2018**, *6* (8), 9979–9989. <https://doi.org/10.1021/acssuschemeng.8b01207>.
- (74) Chapple, A.; Nguyen, L. N.; Hai, F. I.; Dosseto, A.; Rashid, M. H. O.; Oh, S.; Price, W. E.; Nghiem, L. D. Impact of Inorganic Salts on Degradation of Bisphenol A and Diclofenac by Crude Extracellular Enzyme from *Pleurotus Ostreatus*. *Biocatal. Biotransformation* **2019**, *37* (1), 10–17. <https://doi.org/10.1080/10242422.2017.1415332>.
- (75) Stadlmair, L. F.; Grosse, S.; Letzel, T.; Drewes, J. E.; Grassmann, J. Comprehensive MS-Based Screening and Identification of Pharmaceutical Transformation Products Formed during Enzymatic Conversion. *Anal. Bioanal. Chem.* **2019**, *411* (2), 339–351. <https://doi.org/10.1007/s00216-018-1442-7>.
- (76) Lonappan, L.; Rouissi, T.; Liu, Y.; Brar, S. K.; Surampalli, R. Y. Removal of Diclofenac Using Microbiochar Fixed-Bed Column Bioreactor. *J. Environ. Chem. Eng.* **2019**, *7* (1), 102894. <https://doi.org/10.1016/j.jece.2019.102894>.

- (77) Alharbi, S. K.; Nghiem, L. D.; van de Merwe, J. P.; Leusch, F. D. L.; Asif, M. B.; Hai, F. I.; Price, W. E. Degradation of Diclofenac, Trimethoprim, Carbamazepine, and Sulfamethoxazole by Laccase from *Trametes Versicolor*: Transformation Products and Toxicity of Treated Effluent. *Biocatal. Biotransformation* **2019**, *37* (6), 399–408. <https://doi.org/10.1080/10242422.2019.1580268>.
- (78) Ben Younes, S.; Ben Khedher, S.; Zhang, Y.; Geissen, S. U.; Sayadi, S. Laccase from *Scytalidium Thermophilum*: Production Improvement, Catalytic Behavior and Detoxifying Ability of Diclofenac. *Catal. Letters* **2019**, 1833–1844. <https://doi.org/10.1007/s10562-019-02771-1>.
- (79) Apriceno, A.; Astolfi, M. L.; Girelli, A. M.; Scuto, F. R. A New Laccase-Mediator System Facing the Biodegradation Challenge: Insight into the NSAIDs Removal. *Chemosphere* **2019**, *215*, 535–542. <https://doi.org/10.1016/j.chemosphere.2018.10.086>.
- (80) Zdarta, J.; Jankowska, K.; Wyszowska, M.; Kijewska-Gawrońska, E.; Zgoła-Grzeškowiak, A.; Pinelo, M.; Meyer, A. S.; Moszyński, D.; Jesionowski, T. Robust Biodegradation of Naproxen and Diclofenac by Laccase Immobilized Using Electrospun Nanofibers with Enhanced Stability and Reusability. *Mater. Sci. Eng. C* **2019**, *103*, 109789. <https://doi.org/10.1016/j.msec.2019.109789>.
- (81) Kasonga, T. K.; Coetzee, M. A. A.; Kamika, I.; Momba, M. N. B. Assessing a Co-Culture Fungal Granule Ability to Remove Pharmaceuticals in a Sequencing Batch Reactor. *Environ. Technol. (United Kingdom)* **2020**. <https://doi.org/10.1080/09593330.2020.1847204>.
- (82) Camarillo Ravelo, D.; Loera Corral, O.; González-Martínez, I.; Chan Cupul, W.; Rodríguez Nava, C. O. Evaluation of Bezafibrate, Gemfibrozil, Indomethacin, Sulfamethoxazole, and Diclofenac Removal by Ligninolytic Enzymes. *Prep. Biochem. Biotechnol.* **2020**, *50* (6), 592–597. <https://doi.org/10.1080/10826068.2020.1721532>.
- (83) Bankole, P. O.; Adekunle, A. A.; Jeon, B. H.; Govindwar, S. P. Novel Cobiomass Degradation of NSAIDs by Two Wood Rot Fungi, *Ganoderma Applanatum* and *Laetiporus Sulphureus*: Ligninolytic Enzymes Induction, Isotherm and Kinetic Studies. *Ecotoxicol. Environ. Saf.* **2020**, *203*, 110997. <https://doi.org/10.1016/j.ecoenv.2020.110997>.
- (84) Maryšková, M.; Schaabová, M.; Tománková, H.; Novotný, V.; Rysová, M. Wastewater Treatment by Novel Polyamide/Polyethylenimine Nanofibers with Immobilized Laccase. *Water (Switzerland)* **2020**, *12* (2), 588. <https://doi.org/10.3390/w12020588>.
- (85) Asif, M. B.; Van De Merwe, J. P.; Leusch, F. D. L.; Pramanik, B. K.; Price, W. E.; Hai, F. I. Elucidating the Performance of an Integrated Laccase- and Persulfate-Assisted Process for Degradation of Trace Organic Contaminants (TrOCs). *Environ. Sci. Water Res. Technol.* **2020**, *6* (4), 1069–1082. <https://doi.org/10.1039/c9ew01022j>.
- (86) Dalecka, B.; Juhna, T.; Rajarao, G. K. Constructive Use of Filamentous Fungi to Remove Pharmaceutical Substances from Wastewater. *J. Water Process Eng.* **2020**, *33*, 100992. <https://doi.org/10.1016/j.jwpe.2019.100992>.
- (87) Hultberg, M.; Ahrens, L.; Golovko, O. Use of Lignocellulosic Substrate Colonized by Oyster Mushroom (*Pleurotus Ostreatus*) for Removal of Organic Micropollutants from Water. *J. Environ. Manage.* **2020**, *272*, 111087. <https://doi.org/10.1016/j.jenvman.2020.111087>.
- (88) Primožič, M.; Kravanja, G.; Knez, Ž.; Crnjac, A.; Leitgeb, M. Immobilized Laccase in the Form of (Magnetic) Cross-Linked Enzyme Aggregates for Sustainable Diclofenac (Bio)Degradation. *J. Clean. Prod.* **2020**, *275*, 124121. <https://doi.org/10.1016/j.jclepro.2020.124121>.

- (89) Neelkant, K. S.; Shankar, K.; Jayalakshmi, S. K.; Sreeramulu, K. Purification, Biochemical Characterization, and Facile Immobilization of Laccase from *Sphingobacterium Ksn-11* and Its Application in Transformation of Diclofenac. *Appl. Biochem. Biotechnol.* **2020**, *192* (3), pages831–844. <https://doi.org/10.1007/s12010-020-03371-1>.
- (90) Horn, C.; Pospiech, D.; Allertz, P. J.; Müller, M.; Salchert, K.; Hommel, R. Chemical Design of Hydrogels with Immobilized Laccase for the Reduction of Persistent Trace Compounds in Wastewater. *ACS Appl. Polym. Mater.* **2021**, *3* (5), 2823–2834. <https://doi.org/10.1021/acsapm.1c00380>.
- (91) Maryskova, M.; Linhartova, L.; Novotny, V.; Rysova, M.; Cajthaml, T.; Sevcu, A. Laccase and Horseradish Peroxidase for Green Treatment of Phenolic Micropollutants in Real Drinking Water and Wastewater. *Environ. Sci. Pollut. Res.* **2021**, *28*, 31566–31574. <https://doi.org/10.1007/s11356-021-12910-0>.
- (92) Apriceno, A.; Silvestro, I.; Girelli, A.; Francolini, I.; Pietrelli, L.; Piozzi, A. Preparation and Characterization of Chitosan-Coated Manganese-Ferrite Nanoparticles Conjugated with Laccase for Environmental Bioremediation. *Polymers (Basel)*. **2021**, *13* (9), 1453. <https://doi.org/10.3390/polym13091453>.
- (93) Masjoudi, M.; Golgoli, M.; Ghobadi Nejad, Z.; Sadeghzadeh, S.; Borghei, S. M. Pharmaceuticals Removal by Immobilized Laccase on Polyvinylidene Fluoride Nanocomposite with Multi-Walled Carbon Nanotubes. *Chemosphere* **2021**, *263*, 128043. <https://doi.org/10.1016/j.chemosphere.2020.128043>.
- (94) Chong, M. N.; Jin, B.; Chow, C. W. K.; Saint, C. Recent Developments in Photocatalytic Water Treatment Technology: A Review. *Water Research*. 2010, pp 2997–3027. <https://doi.org/10.1016/j.watres.2010.02.039>.
- (95) Ternes, T. A.; Meisenheimer, M.; McDowell, D.; Sacher, F.; Brauch, H. J.; Haist-Gulde, B.; Preuss, G.; Wilme, U.; Zulei-Seibert, N. Removal of Pharmaceuticals during Drinking Water Treatment. *Environ. Sci. Technol.* **2002**, *36* (17), 3855–3863. <https://doi.org/10.1021/es015757k>.
- (96) Ternes, T. A.; Stüber, J.; Herrmann, N.; McDowell, D.; Ried, A.; Kampmann, M.; Teiser, B. Ozonation: A Tool for Removal of Pharmaceuticals, Contrast Media and Musk Fragrances from Wastewater? *Water Res.* **2003**, *37* (8), 1976–1982. [https://doi.org/10.1016/S0043-1354\(02\)00570-5](https://doi.org/10.1016/S0043-1354(02)00570-5).
- (97) Magureanu, M.; Piroi, D.; Mandache, N. B.; David, V.; Medvedovici, A.; Parvulescu, V. I. Degradation of Pharmaceutical Compound Pentoxifylline in Water by Non-Thermal Plasma Treatment. *Water Res.* **2010**, *44* (11), 3445–3453. <https://doi.org/10.1016/j.watres.2010.03.020>.
- (98) Magureanu, M.; Piroi, D.; Mandache, N. B.; David, V.; Medvedovici, A.; Bradu, C.; Parvulescu, V. I. Degradation of Antibiotics in Water by Non-Thermal Plasma Treatment. *Water Res.* **2011**, *45* (11), 3407–3416. <https://doi.org/10.1016/j.watres.2011.03.057>.
- (99) Gopi, C.; Dhanaraju, M. D. Recent Progress in Synthesis, Structure and Biological Activities of Phenothiazine Derivatives. *Rev. J. Chem.* **2019**, *9* (2), 95–126. <https://doi.org/10.1134/S2079978019020018>.
- (100) Padnya, P. L.; Khadieva, A. I.; Stoikov, I. I. Current Achievements and Perspectives in Synthesis and Applications of 3,7-Disubstituted Phenothiazines as Methylene Blue Analogues. *Dye. Pigment.* **2023**, *208*, 110806. <https://doi.org/10.1016/j.dyepig.2022.110806>.
- (101) Gal, M.; Turza, A.; Stoean, B.; Gaina, L.; Cristea, C.; Gal, E.; Lovasz, T.; Porumb, D.; Silaghi-

- Dumitrescu, L. Alternative Procedures for the Green Synthesis of 3,7-Bis(N,N-(2-Hydroxyethyl)Amino)Phenothiazinium Dye. *Stud. Univ. Babeş-Bolyai Chem.* **2022**, 67 (4), 303–314. <https://doi.org/10.24193/subbchem.2022.4.20>.
- (102) Stoean, B.; Gaina, L.; Cristea, C.; Silaghi-Dumitrescu, R.; Branzanic, A. M. V.; Focsan, M.; Fischer-Fodor, E.; Tigu, B.; Moldovan, C.; Cecan, A. D.; Achimas-Cadariu, P.; Astilean, S.; Silaghi-Dumitrescu, L. New Methylene Blue Analogues with N-Piperidinyl-Carbinol Units: Synthesis, Optical Properties and in Vitro Internalization in Human Ovarian Cancer Cells. *Dye. Pigment.* **2022**, 110460. <https://doi.org/10.1016/J.DYEPIG.2022.110460>.
- (103) Tsuchida, R. Absorption Spectra of Co-Ordination Compounds. I. *Bull. Chem. Soc. Jpn.* **1938**, 13 (5), 388–400. <https://doi.org/10.1246/bcsj.13.388>.
- (104) *No Title*.
https://chem.libretexts.org/Courses/Saint_Marys_College_Notre_Dame_IN/CHEM_342%3A_Bio-inorganic_Chemistry/Readings/Purgatory/Chapter_3%3A_Introduction_to_Advanced_Bonding_Theories/3.2_Ligand_Field_Theory/B._Ligand_Field_Theory/B.2._Spectrochemical_Series.
- (105) Silaghi-Dumitrescu, R.; Silaghi-Dumitrescu, I. Hemes Revisited by Density Functional Approaches . 1 The Axial Ligand and the Dioxygen-Peroxo Chemistry. *Rev. Roum. Chim.* **2004**, 49, 257–268.
- (106) Silaghi-Dumitrescu, R. *Metalele În Sistemele Vii*; Presa Universitara Clujeana: Cluj-Napoca, Romania, 2010.
- (107) Attia, A. A. A.; Lupan, A.; Silaghi-Dumitrescu, R. Spin State Preference and Bond Formation/Cleavage Barriers in Ferrous-Dioxygen Heme Adducts: Remarkable Dependence on Methodology. *RSC Adv.* **2013**, 3 (48), 26194–26204. <https://doi.org/10.1039/c3ra45789c>.
- (108) Silaghi-Dumitrescu, R.; Svistunenko, D. A. A.; Cioloboc, D.; Bischin, C.; Scurtu, F.; Cooper, C. E. E. Nitrite Binding to Globins: Linkage Isomerism, EPR Silence and Reductive Chemistry. *Nitric Oxide - Biol. Chem.* **2014**, 42, 32–39. <https://doi.org/10.1016/j.niox.2014.08.007>.
- (109) Silaghi-Dumitrescu, R.; Uta, M. M.; Makarov, S. V. Nitrite Linkage Isomerism in Hemes and Related Complexes - Modulation by Metal, Oxidation State, Macrocycle, and Medium Polarity. *Rev. Roum. Chim.* **2010**, 55 (11–12).
- (110) Silaghi-Dumitrescu, R. Linkage Isomerism in Nitrite Reduction by Cytochrome Cd1 Nitrite Reductase. *Inorg. Chem.* **2004**, 43 (12), 3715–3718. <https://doi.org/10.1021/ic035403p>.
- (111) Mot, A. C.; Bischin, C.; Damian, G.; Attia, A. A. A.; Gal, E.; Dina, N.; Leopold, N.; Silaghi-Dumitrescu, R. Fe(III) – Sulfide Interaction in Globins: Characterization and Quest for a Putative Fe(IV)-Sulfide Species. *J. Inorg. Biochem.* **2018**, 179, 32–39. <https://doi.org/10.1016/j.jinorgbio.2017.10.015>.
- (112) Mot, A. C.; Puscas, C.; Dorneanu, S. A.; Silaghi-Dumitrescu, R. EPR Detection of Sulfanyl Radical during Sulfhemoglobin Formation – Influence of Catalase. *Free Radic. Biol. Med.* **2019**, 137, 110–115. <https://doi.org/10.1016/j.freeradbiomed.2019.04.034>.